Repumping Strontium: from Laser Construction to Repumping in a Magneto-Optical Trap

Zhoumuyan Geng

July 27, 2017

Abstract

This thesis focuses on repumping ultracold strontium (Sr) from metastable triplet states. We describe the construction of two repump External Cavity Diode Lasers (ECDL), construction of the associated laser setup for locking and power distribution, and characterize the repumping performance.

We constructed two ECDLs to drive the $^3P_0$-$^3S_1$ (679 nm) and $^3P_2$-$^3S_1$ (707 nm) transitions in Sr, which can be used to repump Sr atoms from the $^3P_0$ and $^3P_2$ metastable states back to the ground-state. Details on construction elements, building procedures and laser characterization are offered such that an interested reader may follow the content and reproduce a similar ECDL. The two ECDLs were mainly built for the Strontium Perpetual Atom Laser (SrPAL) project.

A setup for locking the two ECDLs and distributing their optical power was constructed. The two ECDLs are currently locked to a high-finesse (99.94% reflectivity for both mirrors) optical cavity using the Pound-Drever-Hall technique. As a cavity is not an absolute frequency reference, the Sr 2D blue MOT in the SrPAL machine is used as the absolute reference to calibrate the locking cavity.

With the two lasers at hand, experiments on the repumping of Sr atoms were performed. First, we scanned the piezo-transducers in the ECDLs to observe the repumping signal and found that only a small intensity, 0.003 mW/cm^2 for the 679 nm laser and 0.03 mW/cm^2 for the 707 nm laser, is needed to saturate the repumping signal in the SrPAL's blue MOT. Then we roughly measured the $^3P_2$-$^3S_1$ and $^3P_0$-$^3S_1$ transition frequencies in ^{84}Sr to be 423913460 (30, sys.) (6, stat.) MHz and 441332834 (30, sys.) (3, stat.) MHz respectively.

The construction of an auxiliary iodine spectroscopy setup will be described in chapter 4. This spectroscopy setup is expected to become a general absolute wavemeter for our lab's lasers.

Contents

1 Introduction **1**
1.1 Laser Diode 1
1.2 External Cavity Diode Laser 3
1.3 Ultracold Strontium 4
1.4 Thesis Overview 6

2 Construction of Repump ECDLs **8**
2.1 Basic ECDL Theory 8
2.1.1 External Cavity and Diffraction Grating 9
2.1.2 Littrow Configuration 12
2.1.3 Mode Hopping 13
2.2 Construction of Homemade ECDLs 13
2.2.1 ECDL Components and Structure 14
2.2.2 ECDL Assembly Procedure 22
2.2.3 Status of the Repump ECDLs 29
2.3 Characterization of ECDLs 30
2.3.1 Free-Running Characterization 30
2.3.2 ECDL Characterization 32
2.3.3 Short-term Linewidth 34
2.4 Slave Laser Construction and Injection Locking 34
2.4.1 Construction of Homemade Slave Laser 35
2.4.2 Injection Locking 36

3 ECDL Locking, Power Distribution and Repumping **38**
3.1 Pound-Drever-Hall scheme 40

3.2 Repump Laser Setup 43
3.2.1 PDH Cavity Locking 44
3.2.2 Beampaths to the SrPAL Machine 46
3.3 Theoretical Aspects of Repumping Effect in Strontium 47
3.3.1 Strontium Blue MOT and Repumping 48
3.3.2 SrPAL Red MOT and Repumping 49
3.4 Characterization of Repumping and Frequency Measurement of the Two Repumping Transitions 50
3.4.1 Characterization of Repumping 50
3.4.2 Measurement of the Two Repumping Transitions 54

4 Iodine Spectroscopy As Absolute Reference 57
4.1 Introduction 57
4.2 Saturated Absorption Spectroscopy 58
4.3 Experimental Setup 60

5 Summary and Outlook 63
5.1 Summary 63
5.2 Outlook 64

List of Figures

1.1 A schematic of the typical structure of the laser diode 1
1.2 Laser diode and diode chip 2
1.3 Two ECDL geometries 3
1.4 Strontium energy level 4
1.5 Vacuum chamber of the Strontium Perpetual Atom Laser 6

2.1 Profiles of different elements in an ECDL in frequency domain . . . 9
2.2 The grating equation 10
2.3 Side view of a holographic grating 11
2.4 First-order diffraction efficiency of a commercial holographic grating 11
2.5 Littrow configuration with a parallel mirror and a good pivot point 12
2.6 Fully equipped ECDLs in two implementation geometries 14
2.7 The grating mount and the old-version base 16
2.8 The grating mount and the new-version base 17
2.9 Top view of the grating mount and the old-version base 18
2.10 Side view of the grating mount and the old-version base 18
2.11 Solidworks simulation of strain and stress distribution 19
2.12 The previous, and the improved grating mount designs 21
2.13 A grating mount with a glued holographic grating and a glued mirror 24
2.14 The power-current curves with, and without an external cavity shown on an oscilloscope 26
2.15 Schematic of the setup for aligning the external cavity 26
2.16 Output polarization of a reasonably well injected polarization maintaining fiber 28
2.17 Current status of the 707 nm ECDL 29

2.18 Free-running λ-T curves for both diodes 31
2.19 Power-Current curves for the free-running diode, the ECDL and the Spec 32
2.20 Final λ-I curves for both ECDLs 33
2.21 Homemade slave laser design 35
2.22 Schematic of basic injection locking geometry 36

3.1 Laser instability 38
3.2 Schematic of basic PDH setup 40
3.3 A cavity's reflection profile, and the relative positions of a carrier and two sidebands with respect to the locking position 41
3.4 A PDH error signal 42
3.5 Schematic of the repump laser setup 43
3.6 The injection-locking path and the cavity-locking path 43
3.7 Locking scheme for the repump ECDLs 44
3.8 Two TEM_{00} modes indicating that both ECDLs are locked 45
3.9 Electronics and the real error signal for PDH locking from an oscilloscope 46
3.10 Relevant energy levels for repumping Sr atoms 48
3.11 The pioneering work of making a BEC only through laser cooling . 50
3.12 The repumping signal from the blue MOT of the SrPAL 52
3.13 Curve of fluorescence vs. the 707 nm laser's power 53
3.14 Curve of fluorescence vs. the 679 nm laser's power curve 53
3.15 Data of the $^3P_2$-$^3S_1$ transition measurement 55

4.1 Pump-probe geometry 59
4.2 An example of the saturated absorption spectroscopy signals 59
4.3 The cold finger and the heated part 60
4.4 The real iodine cell 61
4.5 Schematic of our iodine spectroscopy setup 61

List of Tables

2.1 Part numbers of commercial components in both ECDLs 23

3.1 Optical intensity to saturate the repumping signal in the blue MOT of the SrPAL 51

3.2 The final result of the measurement 56

Chapter 1

Introduction

1.1 Laser Diode

Diode lasers belong to the semiconductor laser category. Although the gain medium of a semiconductor laser is in solid state, semiconductor lasers are classified as a separate type, while a solid state laser conventionally refers to a laser whose gain medium is Ti-Sapphire or Nd:YAG etc.

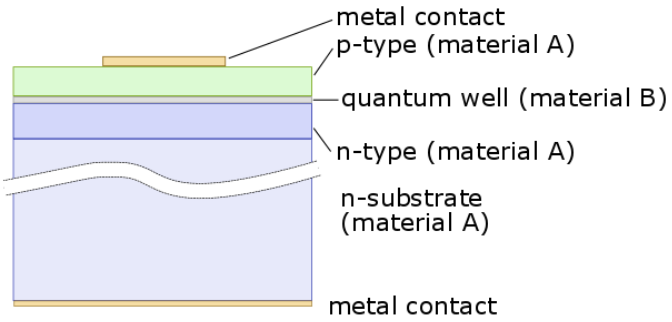


Figure 1.1: A schematic of the typical structure of the laser diode. The quantum well is the intrinsic region for electron-hole recombination. ***Copied from [1].***

A laser diode is essentially a PIN diode (figure 1.1), where PIN stands for Positive, Intrinsic, Negative. The place where photons are produced and confined is the intrinsic region. The positive and negative regions can be regarded as electron and hole reservoirs. When a voltage bias is applied, an electric current consisting of electrons and holes flows into the intrinsic region, where they will

recombine (annihilate). When such an event happens, the electron will re-occupy the energy state of the hole and a photon is emitted. These spontaneously emitted photons are the seed for the following stimulated emission. The positive, intrinsic and negative regions together effectively act as the gain medium.

In the simplest semiconductor lasers the cleaved surfaces of the semiconductor crystal are used as semitransparent mirrors to form a resonator. Without optical coating the reflectivity is determined by the large step in index of refraction between the semiconductor and air. The two "mirrors" are conventionally denoted as the rear facet and the front facet. The rear facet is usually coated with high reflectivity (HR) coating and the transmission of light through the front fact is the laser output. Also, some diodes' front facets are coated with anti-reflection coating (AR) so that those diodes do not have the inner resonator. A resonator built from the outside is required to implement such diodes. As the light is generated and confined within the tiny diode chip (figure 1.2), the tiny beam will diffract once the light is out-coupled through the front facet and thereby expands rapidly. In order to obtain a beam that can propagate long distances without changing its diameter too much, collimation must be performed.

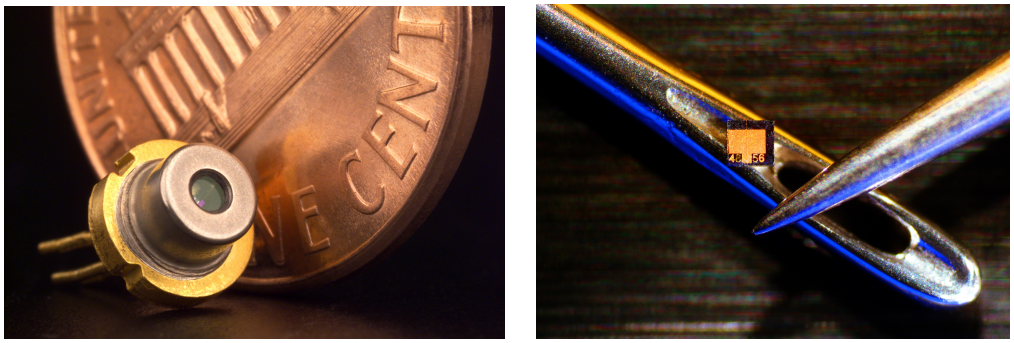


Figure 1.2: Laser diode and diode chip. Compact and cheap. ***Copied from [2, 3].***

For any laser diode, a threshold of electric current exists above which it starts to lase. If the operating current is smaller than the threshold, the optical gain becomes smaller than the loss; when the operating current is turned up, the number of electron-hole recombination sites is increased and lasing starts.

Because they are cheap, compact (figure 1.2) and readily available for ever more wavelengths, laser diodes have become one of the most important light sources in

any quantum gas lab, while expensive, giant and difficult to use dye lasers were used 20∼30 years ago [4].

1.2 External Cavity Diode Laser

In quantum gas experiments, lasers are routinely used for tasks such as laser-cooling atoms, optical pumping, or detection of atoms. Many such applications are associated with driving atomic transitions. A typical relevant transition has a linewidth on the order of several MHz (induced by the electric dipole interaction). In this case, a laser with several hundred kHz linewidth will work satisfactorily.

Due to their compactness, versatility and low price, laser diodes have been widely used in quantum gas experiments. However, as the diode's own cavity has low finesse and is also not sufficiently stable, light from a bare laser diode often spans nanometers in wavelength. In addition, the frequency of a bare diode's output can only be tuned by changing its temperature and operating current, while atomic physics experiments always require GHz tuning range and MHz precision for frequency control.

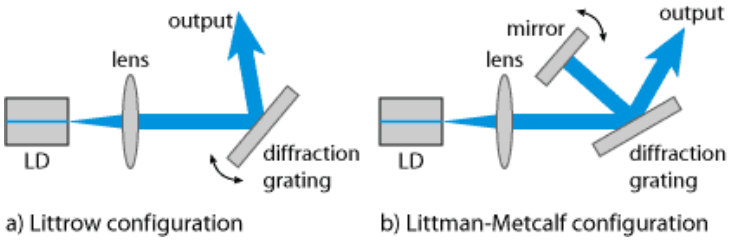


Figure 1.3: Two ECDL geometries. ***Copied from [5].***

In order to overcome these problems, a good method is to implement a tunable external cavity, constructing an External Cavity Diode Laser (ECDL). Two ECDL geometries are commonly used: Littrow and Littmann configurations (figure 1.3). In the Littrow geometry, the external cavity is formed between the rear facet of a laser diode and a diffraction grating. When light hits the grating, one specific frequency component is reflected backwards into the diode chip and the gain is the highest for this frequency component. Other frequency components will be dispersed out of the cavity and because of this loss the laser will not lase at those

frequencies. As the selected frequency is dependent on the grating's relative angle to the diode's output direction and length of the external cavity, an ECDL's frequency can be tuned simply by rotating the grating. In the Littmann geometry, an additional mirror is implemented so instead the mirror is rotated for such tuning. In this thesis work, the Littrow geometry is selected to build two homemade ECDLs to drive the repumping transitions in ultracold strontium gas.

1.3 Ultracold Strontium

Strontium is an alkaline-earth element with two valence electrons in the 5S shell. Different from the alkali elements, this two-electron structure comprises singlet and triplet spin configurations offering many interesting research possibilities. For instance, an optical lattice clock working on the doubly forbidden $^1S_0$-$^3P_0$ transition in ^{87}Sr is currently the best atomic clock human beings ever built [6]; 9/2 nuclear spin of ^{87}Sr offers a platform to study SU(10) symmetry. The relevant electronic structure in strontium is depicted in figure 1.4.

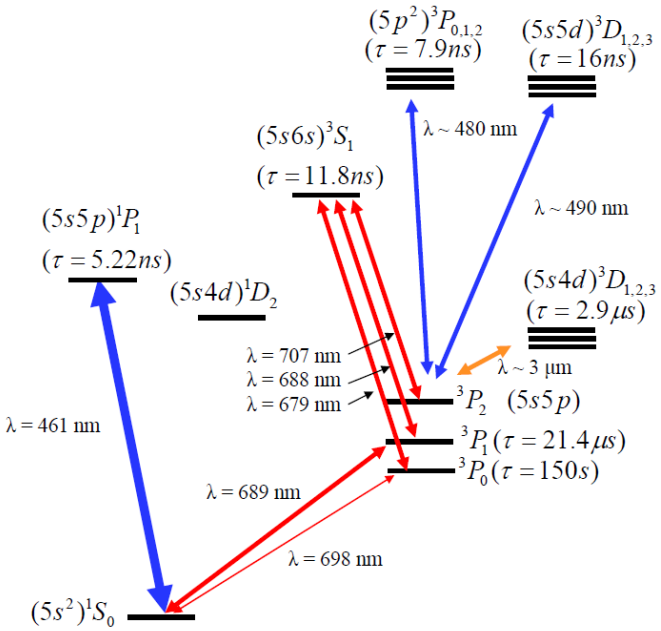


Figure 1.4: Strontium energy level. ***Copied from [7].***

The 461 nm (blue) $^1S_0$-$^1P_1$ transition is strongly electric dipole allowed resulting in a large transition rate (30 MHz). Therefore this blue transition is commonly used in the Zeeman slower and the magneto-optical trap (MOT) for pre-cooling in a strontium gas experiment. However, this transition is not closed. A small fraction of $^1P_1$ atoms in the cooling cycle will not decay to the ground-state but instead to the intermediate $^1D_2$ state then to the $^3P_2$ state. The $^3P_2$ state is metastable with a lifetime of 500 s [8], so this leaking channel introduces loss in the MOT operation. Luckily it does not destroy the MOT as opposed to the alkali element cases, but definitely degrades the atomic density in the MOT.

The (5s5p) ^3P_J states consist of the lowest triplet. In general, transitions from singlet states to triplet states are spin-forbidden. But the $^1S_0$-$^3P_1$ (red, 689 nm) transition is weakly electric dipole allowed because of spin-orbit mixing of the $^1P_1$ and $^3P_1$ states rendering a 7.4 kHz transition linewidth [7]. Previously, scientists demonstrated cooling of Sr atoms down to the recoil limit by operating a red MOT on this transition [9]. Since the maximum deceleration on this red cooling transition is insufficient to slow an atomic beam from a Sr oven, atoms are commonly first slowed by a Zeeman slower and MOT operating on the blue transition, before MOT operation is switched over to the red transition. If a quantum gas is desired, the gas is then loaded into a dipole trap, where evaporative cooling is performed. The transitions from the ground-state to the $^3P_0$ and $^3P_2$ states are doubly forbidden (spin and electric dipole) so that the two states are both metastable. The very high Q factor of the $^1S_0$-$^3P_0$ transition has triggered great interest in frequency metrology on it, thus leading to the development of the optical lattice clock. In contrast, the $^1S_0$-$^3P_2$ transition of Sr is not suited for metrology because of its magnetic sensitivity. However the $^3P_2$ state and the serendipity it brings in the Sr blue MOT has played a very important role in the creation of the first Sr BEC [10].

In our lab, one ongoing project is to build the world's first perpetual atom laser, i.e. the Strontium Perpetual Atom Laser (SrPAL) project (figure 1.5) [11]. The goal is to continuously cool ^{84}Sr atoms through a Zeeman slower, a 2D blue MOT, a red MOT and (possibly) evaporation in a dipole trap into quantum degeneracy, followed by out-coupling atoms from the condensate to form a coherent matter wave beam. The reason for this particular isotope, which has a natural abundance of only 0.56%, is its nice scattering length ($+123a_0$, a_0 is Bohr radius), which is very

well suited for evaporative cooling. In the SrPAL machine, the Zeeman slower and the 2D blue MOT offer pre-cooling, and the red MOT is designed to be a reservoir to replenish the atom laser. But as any near-resonant photon will heat a BEC up and thus destroy it, a "transparency beam" impinges on the red MOT to induce a light shift rendering the atoms transparent to the red cooling light. A BEC may thus be formed within the red MOT under such protection [12]. Also, the 2D blue MOT is spatially separated from the red MOT to keep blue photons away from the BEC (two MOT chambers in figure 1.5). In order to transfer Sr atoms from the top-chamber blue MOT to the lower-chamber red MOT, the blue MOT is designed to be 2D with no cooling light in the vertical axis. So cold atoms in the 2D blue MOT can travel downwards under gravity and a fraction of them will be captured by the red MOT.

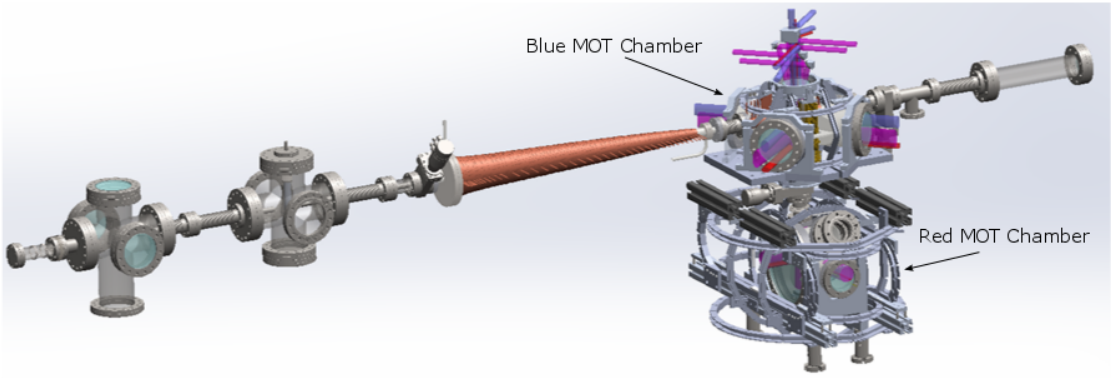


Figure 1.5: Vacuum chamber of the Strontium Perpetual Atom Laser. ***Copied from [13].***

One of the main parts of this thesis work is to build two ECDLs to drive the $^3P_0$-$^3S_1$ and $^3P_2$-$^3S_1$ repumping transitions of ultracold strontium atoms in the SrPAL setup.

1.4 Thesis Overview

The thesis is organized as follows. Chapter 2 describes the basic theory of ECDLs, construction and characterization of two homemade ECDLs, construction of the homemade slave lasers and injection locking. Chapter 3 describes the construc-

tion of the laser setup for locking two ECDLs and for laser power distribution, repumping in ultracold strontium and related experiments. Chapter 4 describes an auxiliary work, the construction of a Doppler-free iodine spectroscopy.

Chapter 2

Construction of Repump ECDLs

Previously, one very urgent task in the SrPAL project was to construct two ECDLs to drive $^3P_0$-$^3S_1$ (679.289 nm) and $^3P_2$-$^3S_1$ (707.202 nm) transitions in strontium, which we wanted to use to repump atoms in the $^3P_0$ and $^3P_2$ states back to the ground-state [14]. The construction work is one of the focuses in this thesis.

In this chapter, the basic aspects of ECDLs will be described, but no theory will be presented. For a detailed theoretical analysis, readers can refer to [15, 16, 17]. The emphasis of the chapter will be on technical issues concerning the construction of the homemade ECDLs and of associated homemade slave lasers, and the characterization on them. In addition, how to injection-lock a slave laser using light from a master laser will be explained.

2.1 Basic ECDL Theory

An ECDL is a tunable laser device with reasonably narrow linewidth, typically several hundred kHz. The core building blocks include a laser diode and a diffraction grating. The tunability of an ECDL's frequency stems from the dispersion of the grating, and the frequency discrimination of the external cavity. Also, optical feedback from the external cavity can significantly reduce the laser's linewidth.

2.1.1 External Cavity and Diffraction Grating

In an ECDL, the external cavity is formed between the rear facet of the laser diode and the reflective diffraction grating. The most important elements in an ECDL include the semiconductor gain medium, the cavity formed by the diode itself and the external cavity. To appreciate how these elements affect the lasing frequency and the linewidth, understanding their "profiles" in the frequency domain is very helpful, as depicted in figure 2.1. "Diode gain" is a measure to describe the laser diode's amplification ability vs. frequency; "Diode cavity" and "External cavity" curves show the cavity transmission vs. frequency; Grating profile, in the ECDL context, always describes the diffraction efficiency of the first-order diffracted light.

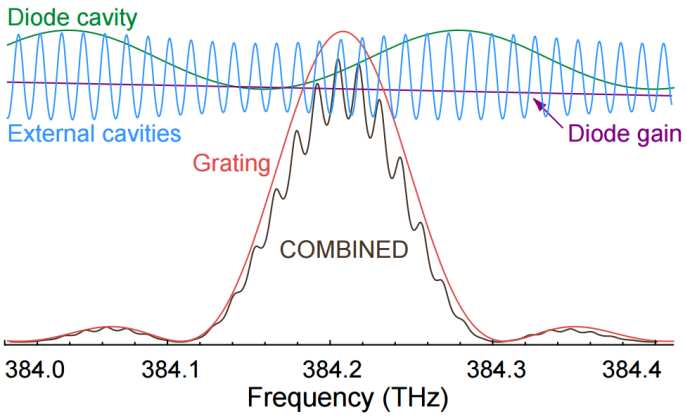


Figure 2.1: Profiles of different elements in an ECDL in frequency domain. ***Copied from [18].***

Introducing the external cavity offers an additional frequency tuning method besides changing the temperature and the electric current of the laser diode, which is to rotate the diffraction grating around a fixed pivot (figure 2.5). In fact, two parameters are tuned simultaneously by this simple rotation: the relative angle between the grating and the diode's beam direction, and length of the external cavity. Each of them affects the lasing frequency in a specific manner and will be explained separately below.

The relative angle of the grating affects the grating's dispersion, shifting the grating profile in figure 2.1 to either left or right. This dispersion is governed by

the grating equation:

$$d(\sin\alpha + \sin\beta) = m\lambda \tag{2.1}$$

where α is incident angle, β is diffracted angle, m is diffraction order, d is spacing. The first-order diffracted light ($m = 1$) is essentially back-reflected into the laser diode. The wavelength of the reflected light is determined by the formula: $\lambda = 2d\sin\alpha$. In fact, the spectrum of the reflected light spans a finite range centered at this value. Therefore, only these frequency components can resonate within the external cavity. Other frequency components are diffracted into other directions and escape from the cavity. Finally the selected resonating frequency will dominate in the ECDL. In conclusion, the grating's dispersion only enables specific frequency components to lase, and this dispersion can be shifted by tuning the relative angle between the grating and the diode's beam direction.

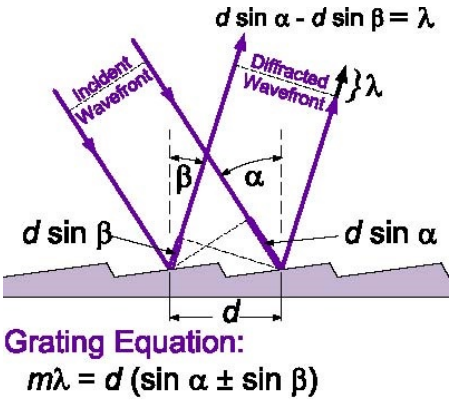


Figure 2.2: The grating equation. Notice that though a ruled grating is used as an example here, this equation holds for any type of grating. *Copied from [19].*

The external cavity's length determines its longitudinal modes and thus affects the ECDL's frequency. In general, a cavity only allows light to resonate whose half wavelength times any integer is equal to the cavity length. Changing the cavity's length will directly shift those modes in the frequency domain. For example, when the cavity becomes longer, all allowed modes will shift to the lower frequency region, and vice versa. As shown in figure 2.1, the external cavity has a much sharper profile than the grating. So on top of the grating profile, the cavity's mode closest to the center of the grating profile will be significantly amplified.

At last, the total effect of gain profile, intra-cavity profile, grating profile,

and external cavity profile determines the final lasing frequency, as shown in the combined curve in figure 2.1.

As mentioned above, two tunable parameters are integrated into one tuning "knob", i.e. the rotation of the grating along a fixed pivot. Mode hopping occurs if shifting the grating profile is not synchronized with shifting the cavity profile. In addition, a longer external cavity can yield narrower intrinsic laser linewidth, but its mechanical stability and mode-hop-free tuning range may be accordingly reduced [20]. So a trade-off must be considered in the design phase of an ECDL.

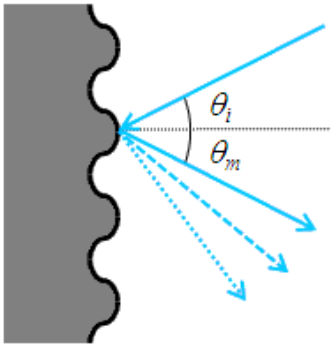


Figure 2.3: Side view of a holographic grating. ***Copied from [21].***

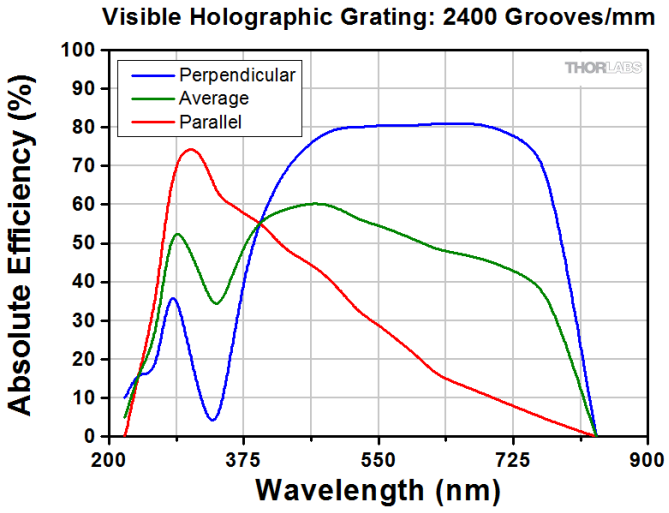


Figure 2.4: First-order diffraction efficiency of a commercial holographic grating. "Perpendicular" and "Parallel" polarization directions are defined with respect to the grating lines. "Average" is simply the average of blue and red curve. ***Copied from [21].***

As for the choice of diffraction grating, the holographic type (figure 2.3) can be selected for convenience. A holographic grating is manufactured using two lasers' interference to create periodic pattern. The advantage is that the variation of the periodicity is significantly reduced, and each specific holographic grating can work for a wide spectral range. However a drawback is that the first-order diffraction efficiency is accordingly reduced. In contrast, a ruled (blazed) grating can offer maximum efficiency for a specific wavelength. But a ruled grating is produced by machining, so periodicity errors occur. Polarization of the light incident on a holographic grating is an important issue, as illustrated in figure 2.4, since the first-order diffraction efficiency of two polarizations greatly differ. For ECDLs, a lower first-order diffraction efficiency is often desired as the resultant optical power buildup in the diode's intra-cavity is reduced and the lifetime of the diode does not suffer too much. In our two repump ECDLs, the "parallel" situation is used for both, reducing for our wavelengths the reflectivity compared to the "perpendicular" situation.

In the two repump ECDLs, reflectivity of the grating is estimated to be 10% according to figure 2.4. The rear facet of the laser diode is assumed to be 99% reflective.

2.1.2 Littrow Configuration

An ECDL is either in the Littrow configuration or in the Littmann configuration. In our design, we choose the Littrow configuration for its simpler structure, sufficient linewidth reduction through the external cavity, and the relatively higher output power.

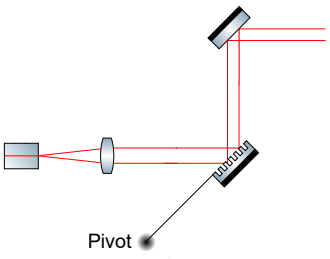


Figure 2.5: Littrow configuration with a parallel mirror and a good pivot point. The geometry in the figure is used in our ECDLs.

The Littrow configuration is pretty straightforward. A diffraction grating is placed right after the laser diode and the collimating lens. In this geometry, the laser's wavelength is determined by the Littrow angle $\lambda = 2d \sin\theta$, so the wavelength can be tuned by rotating the grating. Laser output is the zeroth-order diffracted beam, which is the "mirror reflection" of the grating. If the grating is rotated, the output beam direction also changes causing problems for fiber coupling. In order to lessen this drawback, a parallel mirror is implemented that moves together with the grating (figure 2.5).

2.1.3 Mode Hopping

Mode hopping occurs when an ECDL's frequency is tuned continuously by a piezo-transducer (PZT). The reason is that the grating profile center, previously choosing one longitudinal mode, moves closer to another adjacent mode when the grating is moved such that this adjacent mode becomes dominant. This happens when shifting the cavity profile and shifting the grating profile are not synchronized when the grating is rotated. To reduce mode hopping, the two moving paces have to be synchronized as much as possible, which can be achieved by carefully choosing a good pivot point. According to [22], the optimized mode-hop-free pivot is the intersection of the grating surface and the front facet of the diode. But engineering constraints limit our choice. A pivot with a rotation arm parallel to the grating can still offer good mode-hop-free range (figure 2.5).

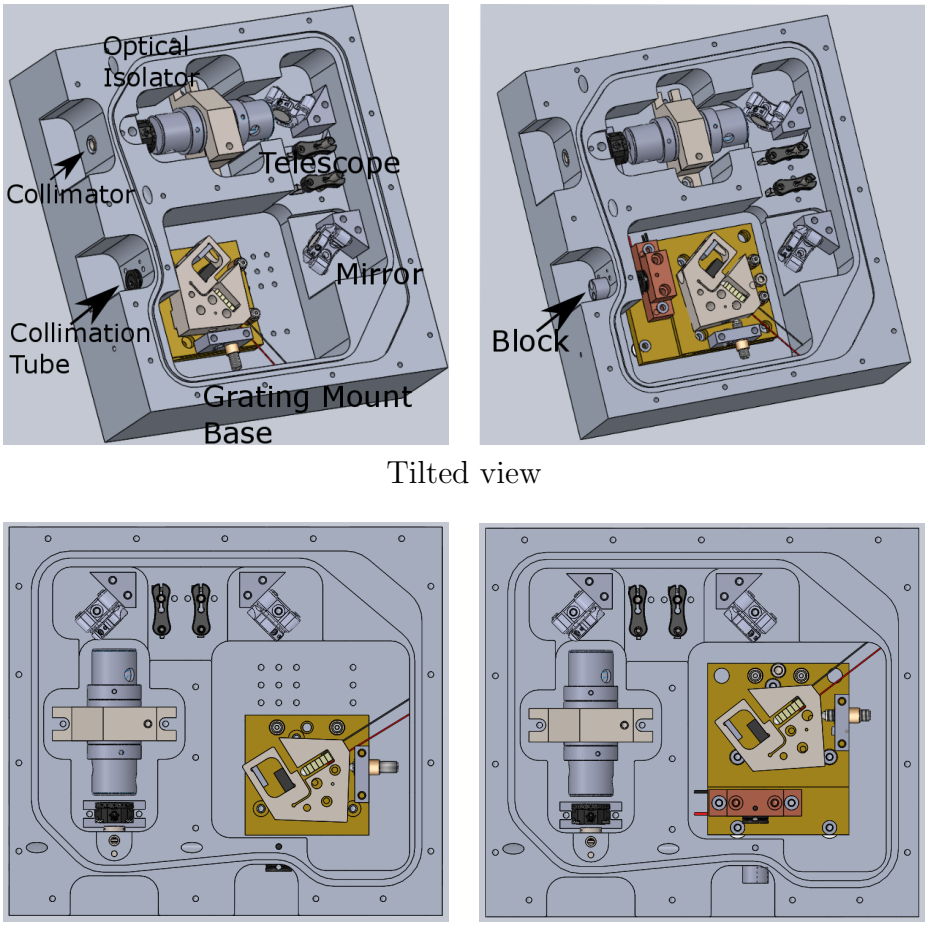
In our design, two pivots coexist: a rough-tuning pivot and a fine-tuning pivot. The rough-tuning pivot is only used to align the external cavity to an angle that roughly offers the wanted lasing wavelength. Once it is fixed and bolted, no touching is allowed. The fine-tuning pivot gives good precision to control the frequency through the PZT. Mode-hop-free design is considered in the fine-tuning pivot as in figure 2.5.

2.2 Construction of Homemade ECDLs

This section provides a detailed description about construction of our homemade ECDLs.

2.2.1 ECDL Components and Structure

In our design, the ECDL's structure consists of six parts: housing, grating mount and base, two mirrors, a telescope, an optical isolator and a half-waveplate (figure 2.6).



(a) First geometry (b) Second geometry

Figure 2.6: Fully equipped ECDLs in two implementation geometries in tilted, top views. The first geometry is used in the 707 nm ECDL; the second geometry is used in the 679 nm ECDL. Two geometries support two different schemes for temperature stabilization, which is explained in text.

Housing

The main feature of the housing is its massive size and weight. The dimension is 240 mm × 220 mm × 70 mm. The housing and lid are made of aluminum, resulting in a weight of around 8 kg. With such a thick and heavy housing, the ECDL should be insensitive to acoustic vibration and thermal fluctuations, resulting in better decoupling from the environment.

Depending on how the temperature is stabilized, two different geometries (with two different designs for the base) are used in our ECDLs (figure 2.6).

The first geometry, which features the use of an old-version base, can only stabilize the ECDL's temperature higher than the room temperature because a cartridge heater is used to warm up the whole housing. Two NTC thermistors are used, one for error-signal generation and the other for temperature readout. The collimation tube for the laser diode is plugged and fixed in the housing's side wall with the thermistors and the cartridge heater positioned nearby. This geometry is currently used in the 707 nm ECDL as the diode's free-running wavelength becomes closer to the target wavelength at a higher temperature. The 679 nm laser diode, however, favors a temperature lower than the room temperature, so using the cartridge heater is not an option. Obviously, it is also difficult to cool down the entire giant housing by a thermal-electric cooler (TEC).

Therefore, the second geometry, which features the use of a new-version base, was conceived and now used in the 679 nm ECDL. In this geometry, the collimation tube is no longer plugged into the housing, but instead in a copper mount which is bolted on the new-version base (figure 2.8). A TEC is inserted between the base and the housing to stabilize the temperature of the copper mount, the grating mount and the base. Indeed, it seems more convenient to just stabilize the copper mount. But stabilizing them together can make it more resistive to thermal fluctuation. The huge housing acts as a heat sink for the TEC. However, we observed that the housing was heated to around 30 °C due to too much heat dumping from the TEC, which resulted in an offset for temperature stabilization. To solve the problem, water cooling on the housing was employed. In addition, as the operating temperature is lower than the room temperature, water condensation on the laser diode and optics may occur. Our solution was to send and vent a constant nitrogen flow into the housing. In order to minimize the induced thermal

fluctuation from the nitrogen flow, the gas pipe is positioned on the side furthest from the collimation tube and the gas flow is monitored (RMA-1 flowmeter) and kept very low (0.1 SCFH[1]). The hole in the housing side wall in which the fiber collimator is plugged in the first implementation geometry must be blocked as a slow venting is needed.

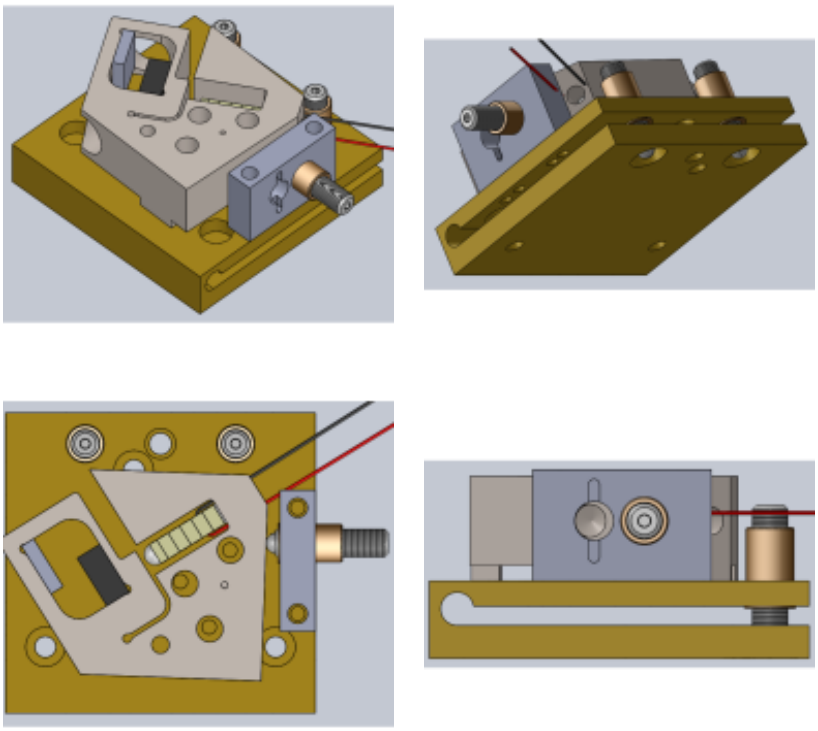


Figure 2.7: The grating mount and the old-version base, used in the first geometry (the 707 nm ECDL).

Grating Mount and Base

The grating mount and base are at the core of our ECDL design. The grating uses the Littrow configuration with a parallel mirror as described in section 2.1. We have two designs of the base: the old-version and the new-version (figure 2.7 and figure 2.8), which are used in the 707 nm ECDL and the 679 nm ECDL respectively. The new-version base is the modification of the old-version base with

[1]SCFH stands for Standard Cubic Feet per Hour.

an elongated bottom to hold a copper mount. The corresponding two implementation geometries are already explained above. The base is fixed by bolting it on a threaded-hole matrix in the housing. In the first geometry the old-version base has smaller size and the length of the external cavity can be changed by choosing different bolting holes. In the second geometry the new-version base has a larger size covering the whole area, which disables this adjustment. The grating mount is placed on the upper layer of the base with a rigid pivot.

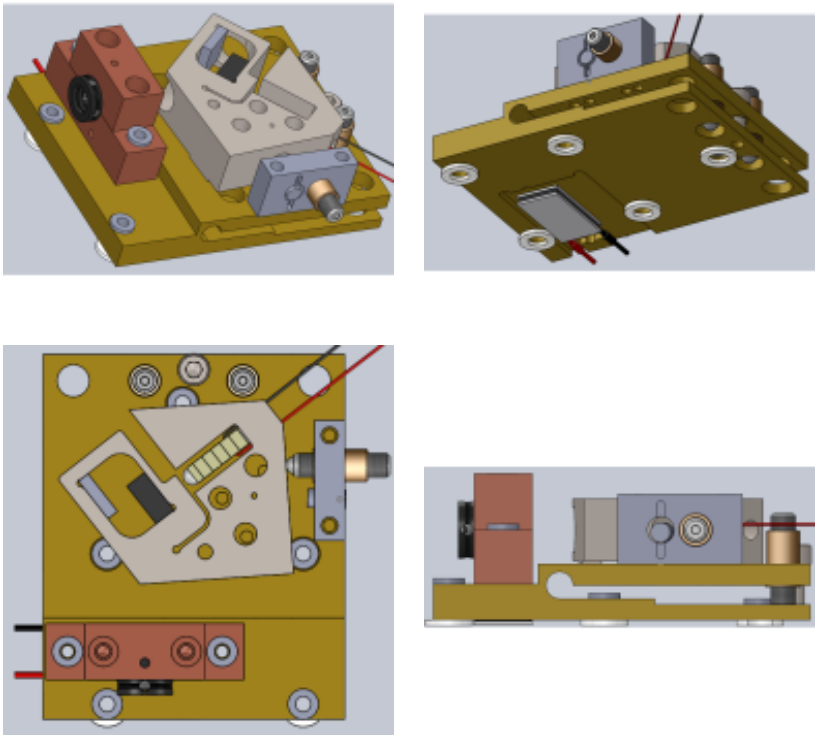


Figure 2.8: The grating mount and the new-version base, used in the second geometry (the 679 nm ECDL).

In our design, two rotating pivots coexist. The first is the rough-tuning pivot. This pivot offers 50 GHz tuning steps. This large step results from the mode-hopping caused by the imprecision of manually tuning the side-tuning screw. We cannot adjust the ECDL's frequency in a deterministic way with this tuning screw better than these steps, so only rough alignment can be achieved to pull the laser's wavelength near the target wavelength. The fine-tuning pivot is designed to be

mode-hop-free. It is manufactured by cutting a channel into the grating mount's flexure to create a rotating arm. A PZT is used to push the arm to fine-tune the grating, which can offer several GHz tuning range. As a PZT can only push the arm forward, the PZT's offset voltage should be set half of its maximum during alignment of the cavity so that fine-tuning can reach both forward and backward displacements. As we used a laser diode without AR coating, mode competition and thus multi-mode operation appeared when the PZT's offset voltage was continuously tuned. This problem can be solved by applying a feedforward signal onto the diode current which was confirmed by manually adjusting the diode current while tuning the PZT. Currently even without feedforward, frequency tuning is smooth within a 1 GHz range by solely touching the PZT.

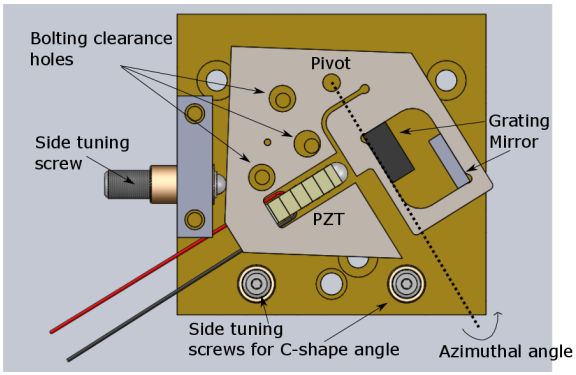


Figure 2.9: Top view of the grating mount and the old-version base. Notice the azimuthal angle for aligning the external cavity.

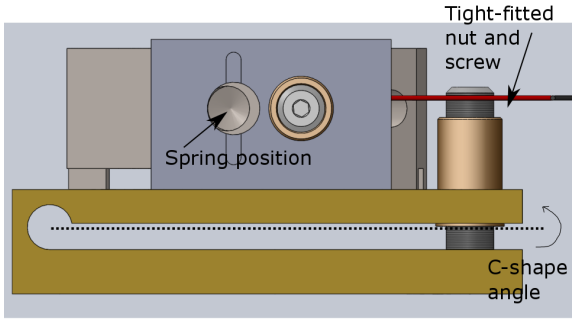
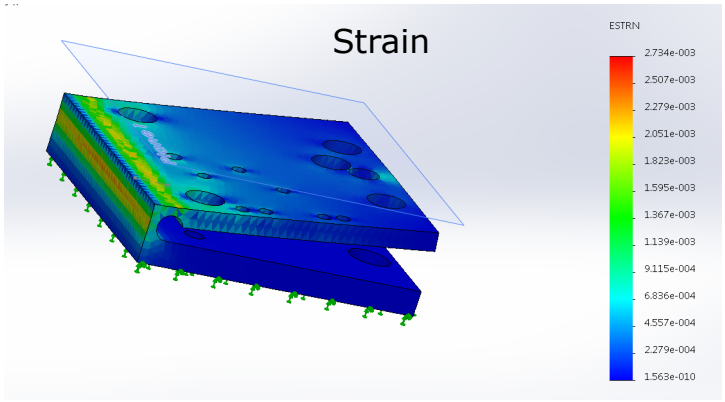


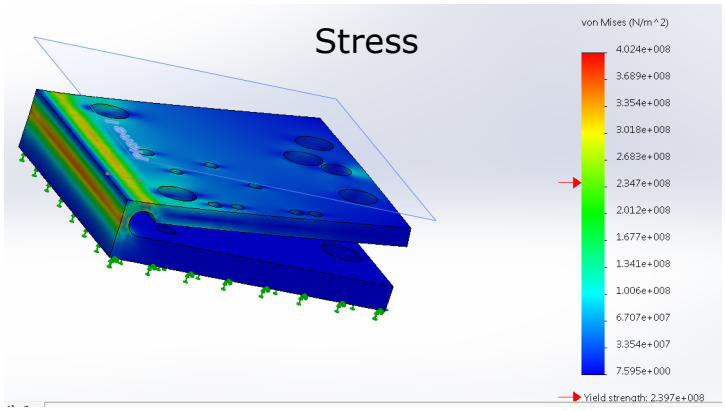
Figure 2.10: Side view of the grating mount and the old-version base. Notice the C-shaped angle for aligning the external cavity.

Alignment of the external cavity is carried out by tuning two angles: the az-

imuthal angle of the grating mount along the rough-tuning pivot, and the opening angle of the C-shaped "mouth" (figure 2.9 and figure 2.10). The azimuthal angle is tuned by a side fine-tuning screw to push the grating mount in or out. A spring is added to facilitate this tuning. The C-shaped angle is tuned using two fine-thread screws and nuts (table 2.1). The nuts are tight-fitted into the upper layer of the base. When the base is bolted and the two fine-thread screws are pressing down, the tight-fitted nut will be pushed up, lifting the upper layer of C-shaped to open up the C-shaped "mouth". This relies on elastic deformation enabling repetitively opening and closing the "mouth". The tuning range, however, is limited. Also, initially the C-shaped layers must be deliberately bended inwards to induce plastic deformation such that the "mouth" is initially closed a bit.



(a) Strain Distribution



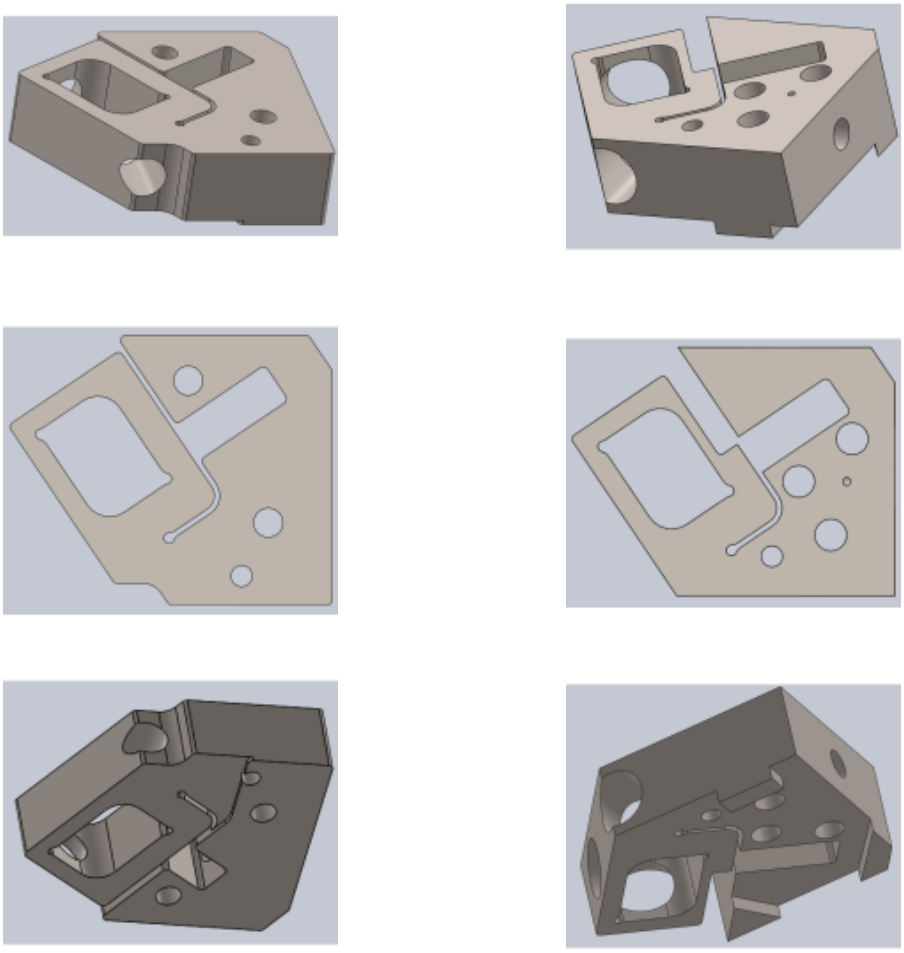
(b) Stress Distribution

Figure 2.11: Solidworks simulation of strain and stress distribution when the C-shaped angle is increased.

Bolting the grating mount on the upper layer of the base may introduce an engineering problem. When the C-shaped angle is increased, some strain may appear in the upper layer, deforming it and thus making it not flat. If this occurs, the grating mount may not sit stably. Therefore, the base is designed such that when the C-shaped "mouth" is lifted strain and stress in the area holding the grating mount are reduced (figure 2.11). But unfortunately, there is still a small but finite strain and stress on the edge of this region. So further improvements should be considered in the future.

As described above, the collimation tube in the 679 nm ECDL is plugged into the copper mount. Therefore instead of stabilizing the temperature of the whole housing, only the temperature of the base, the grating mount and the copper mount is controlled. In addition, plastic spacers and plastic inserts must be used to bolt the base into the housing, in order to thermally separate the heat sink (the housing) and the stabilized part.

The current grating mount is based on the previous design [15] with three upgrades (figure 2.12). First, the old bolting clearance holes cannot reach the correct Littrow angles for both repumping transitions, so they are re-positioned. The holes' diameter is also increased to obtain a greater tuning margin. Second, the previous flat bottom is changed to three points to increase the mechanical stability. Third, the overall size is reduced to save more space for cables. Also, the rotating arm is made lighter so that its intrinsic mechanical resonance frequency becomes higher, which increases the PZT feedback bandwidth for laser locking.



(a) The previous grating mount design (b) The improved grating mount design

Figure 2.12: The previous, and the improved grating mount designs.

Other Components

Mirrors provide sufficient degrees of freedom to control the optical path guiding light through the optical isolator and coupling light into a fiber.

The telescope transforms the beam profile from elliptical, which is the output shape after the collimation lens, to round. We can reach 82% fiber coupling efficiency through a combination of a 4.5 mm fiber collimator and a telescope, which is made of a 40 mm lens and a -25 mm lens to reduce beam size along the fast axis. However, this maximum is very sensitive to mis-alignment, while a 70%$\sim$80% efficiency is much easier to reach.

The optical isolator is used to prevent any undesired etalon accidentally formed between external optics and the ECDL, which may ruin the optical feedback of the external cavity.

A half-waveplate accompanies the use of a polarization maintaining fiber. Only when the polarization of the incident light on the fiber is along a specific direction can it be maintained during propagation through the fiber. The half-waveplate is used to make the match.

2.2.2 ECDL Assembly Procedure

In the building phase, the most annoying issue is that once a mistake or an unexpected problem appears, all the previously finished parts may have to be dissembled, which can be time-consuming. So a good set of assembly procedures is very helpful. In this subsection, a reasonable set of assembly procedures is provided.

Step 1

The first and also the foremost step is to literally gather **everything** needed, including commercial parts and homemade parts, the latter including the housing, the grating mount and the base, two mirror mount blocks, a homemade clamp for the optical isolator, and a waveplate base (figure 2.6).

Table 2.1: Part numbers of commercial components in both ECDLs.

Item	679 nm	707 nm
Laser Diode	QL68J6SA	HL7001MG
Optical Isolator	IOT-5-670-VLP	IO-5-730-HP
Cartridge heater/TEC	H050-15-24-01	ET-031-10-13-RS
Thermistor	B57861S103F40	
Collimation Tube	LT230P-B	
Collimation Lens	C330TMD-B	
Holographic Grating	GH13-24V	
Grating Mirror	ME05S-P01	
Fine Screw	F25US100	
Nut	F25USN2P	
Mirror Mount	POLARIS-K05	
Dielectric Mirror	BB05-E02-10	
Waveplate	Customized by Altechna	
Waveplate Mount	BB05-E02-10	
Fiber Collimator	60FC-4-A4.5-02	
Polarizing Maintaining Fiber	P3-630PM-FC-2	

For homemade components like the housing and the grating mount, it always takes weeks for the mechanical workshop to manufacture them. Unexpected delays and manufacturing defects may also occur from time to time, meaning some extra time will be spent on waiting or doing some machining by oneself. So making an order in advance is essential to save as much time as possible.

For commercial parts, not everything is always available at anytime, especially the very expensive ones like optical isolator and highly customized ones like waveplates. Purchase and delivery may take quite some time, even many months. So purchasing in advance is also important. A good plan can save a lot of time.

In addition, it also takes some effort to tune the homemade electronics to an

ideal condition. The preparation phase always occupies the most time.

Table 2.1 shows the part numbers of commercial components used in the two ECDLs.

Step 2

With all components at hand, some other preparation work has to be done.

The first is to assemble a collimation tube with the laser diode mounted and collimated. The part number of the tube we regularly use is LT230P-B from Thorlab. A newly bought tube has a default 4.5 mm lens screwed inside. But for both diodes used in the repump ECDLs, we found that a 3.1 mm lens could offer better coupling into a 4.5 mm fiber collimator. Therefore this replacement should be done. Additionally, the collimation lens must be glued once the collimation is finished to guarantee good stability.

The second is to glue the holographic grating and the parallel mirror on the grating mount, and to install the PZT, as in figure 2.13.



Figure 2.13: A grating mount with a glued holographic grating and a glued mirror.

The third includes aligning the optical isolator and tuning the collimation lens in the fiber collimator for higher light-fiber coupling efficiency.

Step 3

This step contains the characterization of the free-running laser diode, and the alignment of the optics in order to couple the laser beam into the fiber. There is no need to mount the telescope and the optical isolator at this stage.

The tiny laser diode is the core element of the massive ECDL, so it is necessary to have some basic characterization of its properties such as power vs. electric current relation and lasing wavelength vs. temperature relation.

The collimation tube and fiber collimator ought to be mounted first. The fiber collimator can be inserted in the ECDL housing and held in place by a set screw, while for the collimation tube a layer of thermal paste must cover it evenly before plugging and fixing.

The next step is to bolt the base on the housing and put the grating mount onto it with the dowel (rough rotating pivot) through the holes foreseen for it in the mount and the base. If the new-version base is used, the TEC and plastic spacers should be inserted between the base and the housing.

The next step is to switch on the laser diode and to align the mirrors to couple the light into the fiber. Switching on the laser current must be done with great care to feed in an electric current on the correct scale according to the diode's specification. If much larger operating current is applied, the laser diode may be permanently damaged. In order to facilitate mirror mounting and beam alignment, a handheld laser (Thorlab HLS635 in our case), which injects light from the other side of the fiber to provide a reference beam, is highly recommended. Notice that fiber coupling is not necessary to be optimized at this step.

Finally, **re-checking** the bolting of everything must be performed. In fact, tightening and bolting should be checked from time to time as optics are extremely sensitive to mis-alignment and even a small touch can make a difference. The goal is to make the ECDL vibration-proof.

Step 4

This step is dedicated to the alignment of the external cavity, which is the most essential step of the construction. Beforehand, the PZT offset voltage should be turned to half of its maximum value so that there is sufficient increasing/decreasing margin.

The signature of successful alignment of the external cavity is a reduced lasing threshold, and a Power-Current (P-I) curve with a lower slope (figure 2.14). In order to monitor the P-I curve in real time, a simple setup as in figure 2.15 can be utilized. We used a function generator to modulate the laser current around

the threshold, and a photodetector (PD) to monitor the modulated optical power. By sending the modulated current signal and the PD signal into port 1 and 2 of an oscilloscope, P-I curve will appear in the scope's X-Y mode. Notice that the modulation must cross the laser threshold.

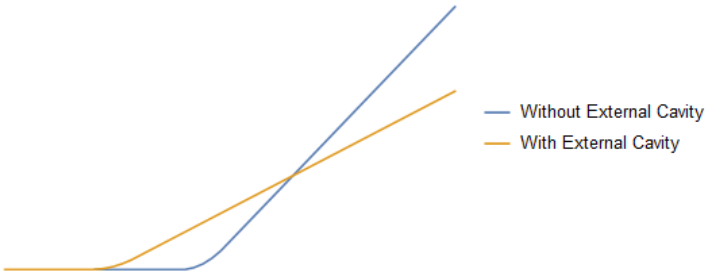


Figure 2.14: The power-current curves with, and without an external cavity shown on an oscilloscope.

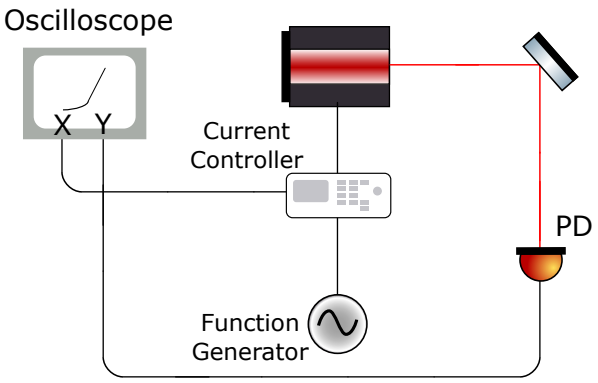


Figure 2.15: Schematic of the setup for aligning the external cavity.

The next step is to rough-align the cavity. By positioning a piece of white paper right after the grating mount, two beam spots can be seen: a laser output spot, and a reflection spot from the diode's front facet. The job is to overlap the two spots by adjusting the azimuthal and C-shaped angles. When they are overlapped, the spot will become brighter due to a smaller lasing threshold. Then,

the fine-alignment should be performed by gently tuning the two angles while monitoring the real-time P-I curve. The most reduced threshold current suggests the optimized alignment. After the alignment, the laser wavelength should differ from the free-running wavelength, and it also becomes tunable. Therefore, now the Littrow angle can be tuned by gently rotating the azimuthal angle. In addition, laser current and temperature are also important parameters because they affect the intra-cavity length. Therefore, characterization of the ECDL must be carried out to check if the combination of the grating position and temperature can center the target wavelength to the mode-hop-free range (figure 2.20). Some iterations may be needed in this process.

Finally, the grating mount must be bolted to ensure reasonable resistance towards external perturbation. Notice that this bolting may misalign the external cavity. So it should be done very carefully.

Step 5

This step is dedicated to installing the telescope and the optical isolator to optimize the fiber coupling efficiency and to get rid of any accidentally formed undesired etalon.

The telescope is installed as follows. First, a piece of soft tape such as PVC electric tape should cover the area of the telescope. Because fixing is through vertical pressing, a soft cushion can both protect optics and keep them stable. As described above, a telescope is made of two lenses. For convenience one can fix the first lens and only align the second. In the two repump ECDLs, two lenses with 40 mm and -25 mm focal length are used to reduce the beam size along the fast axis. A $\sim$75% fiber coupling efficiency is sufficient and it is unnecessary to pursue the ultimate optimum efficiency ($\sim$82%) as it is extremely sensitive to alignment.

The optical isolator is easy to install, which is done by simply plugging it in a homemade mount and bolting it onto the housing. The only concern in practice is that an optical isolator ($\sim$2000 euros) is magnetic so great care must be taken not to smash it on an optical table, whose surface is also magnetic..

Step 6

The last step is to inject the polarization maintaining fiber with the correct polarization, which is done using a half-waveplate and a commercial polarization

analyzer (SK010PA-VIS).

Fiber coupling is integrated in our ECDL for better stability. A fiber collimator is plugged in the side wall of the housing. As polarization of the laser can only be maintained in specific directions, a half-waveplate is used to rotate the polarization to make the match.

The analyzer depicts the polarization state on a Poincaré sphere. If the polarization of the incident light does not match the polarization maintaining axes of the fiber, the polarization state moves around and draws a circle on the Poincaré sphere when perturbation is introduced on the fiber. The job is to rotate the half-waveplate to converge the circle to a point. $\Delta\eta$ in figure 2.16 represents the radius of the circle, and a perfect polarization maintained state corresponds to $\Delta\eta = 0$.

A reasonably well polarization maintained fiber corresponds to $\Delta\eta < 1$ as in the figure. A more detailed description of this particular polarimeter's working principle can be found in its specification.

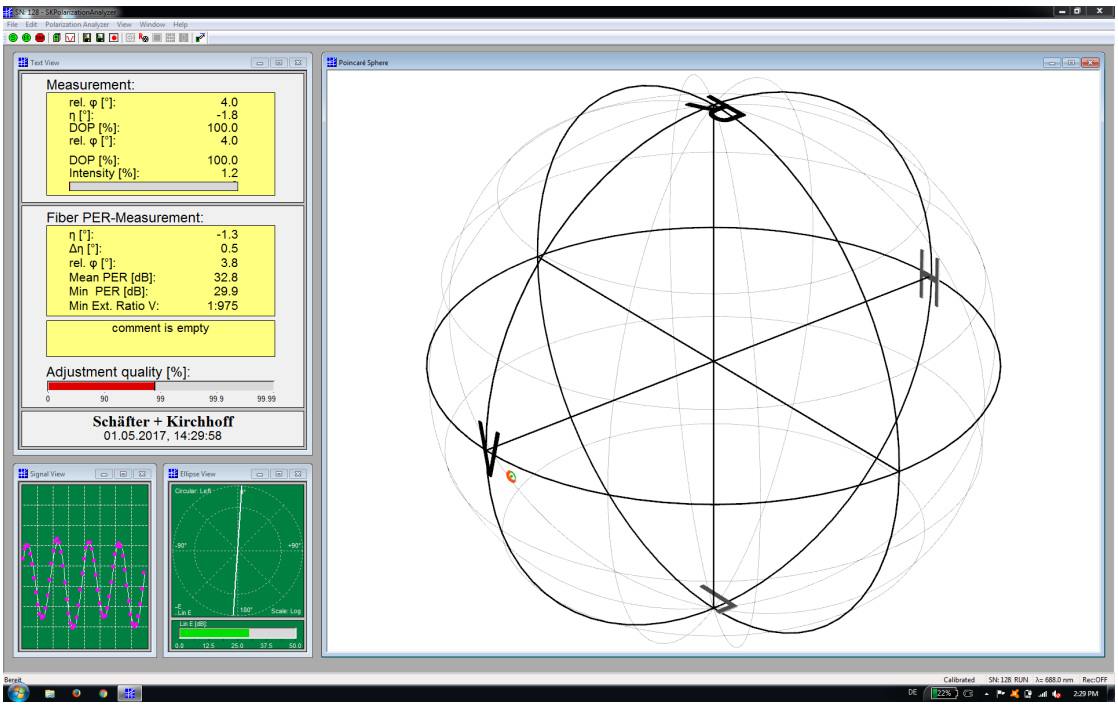


Figure 2.16: Output polarization of a reasonably good injected polarization maintaining fiber.

2.2.3 Status of the Repump ECDLs

Currently the two ECDLs are lying on a shelf above an optical cavity for locking. Each ECDL is sitting in a box made of acoustic absorbing foam (black piece) with a polystyrene lid (white). The foam can absorb acoustic vibration and offer thermal insulation. The polystyrene lid can provide much better thermal insulation, which is important for the 707 nm ECDL because it is stabilized at 30 °C. Without this lid, thermal dissipation is large and the temperature cannot be stabilized due to huge fluctuation. Unfortunately, the laser diode in the 707 nm ECDL degraded in January with the output power dropping from 10 mW to 2.5 mW at 52 mA. We assume the reason is the long-time high current operation. We then turned down the current (now 44 mA) to give just enough power (2 mW) for the PDH locking and injection locking. So far, no further degradation has been observed.

For the 679 nm ECDL, water cooling was integrated onto the ECDL housing as explained in this section. The 679 nm laser diode also degraded. Sadly this diode eventually died. So we replaced it and rebuilt the ECDL. Luckily the optical power at a lower electric current is still sufficient for most experiments, thus no 679 nm slave laser has been implemented. Its operating temperature now is 19 °C. The operating current and power are 38 mA and 6 mW respectively, measured after the fiber.



Figure 2.17: Current status of the 707 nm ECDL. The 679 nm ECDL is in the same condition.

2.3 Characterization of ECDLs

The reason for characterization is to have a better control over the laser's properties, check whether the external cavity is aligned properly, and determine the appropriate operating temperature and electric current.

Characterization should be carried out on both the free-running laser diode and the ECDL. Free-running characterization consists of a Power-Current (P-I) curve, and a Wavelength-Temperature (λ-T) curve at a fixed current. ECDL characterization includes a P-I curve from the fiber output and a λ-I curve.

2.3.1 Free-Running Characterization

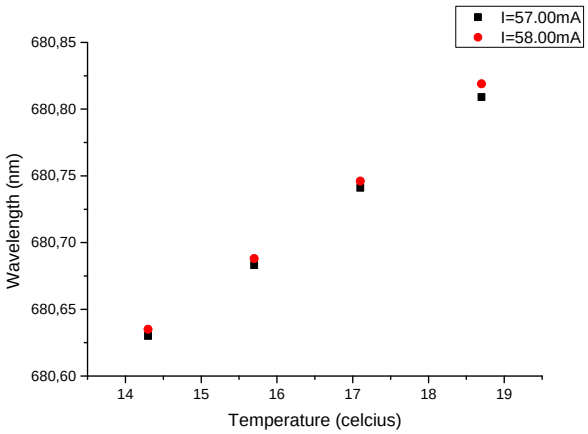
The main purpose of the free-running characterization is to find a proper diode temperature for the target wavelength and to document its actual P-I curve to compare it with the datasheet.

The diode's temperature can affect the intra-cavity's length. Typically, the higher the temperature, the higher the free-running wavelength. The reason is that the refractive index of the gain medium changes when its temperature varies. So equivalently the intra-cavity's length is changed and the longitudinal modes are shifted. Ideally, the temperature for an ECDL should be chosen such that the free-running wavelength centers at the target wavelength. However from figure 2.18, a 5 °C difference only corresponds to a small frequency shift. So if the target wavelength is far away, an extremely high or low temperature is required which is not practical. Usually, once the temperature is sufficiently high or low, grating dispersion is already able to give the correct lasing wavelength. For instance, our 707 nm diode is estimated to emit 707 nm light at 47 °C for free-running operation. But in fact when this diode's temperature is higher than 28 °C, the grating dispersion can already offer the right lasing wavelength

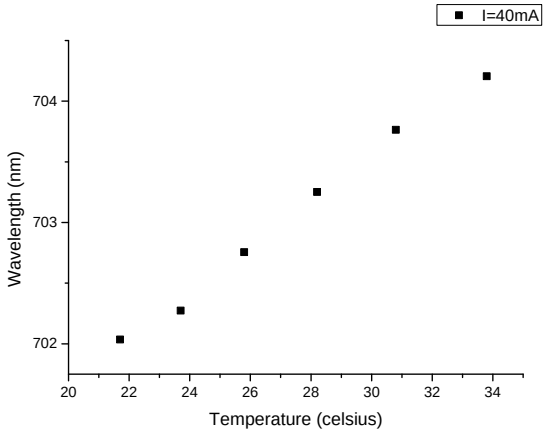
Figure 2.18 shows λ-T curves for both diodes. Both curves illustrate that the central wavelength shifts to higher wavelength region when temperature is increased. Therefore, the 707 nm ECDL needs heating while the 679 nm diode favors a lower temperature. Our temperature controller offers a 12 °C to 35 °C tuning range. We finally found that 30 °C for the 707 nm ECDL and 19 °C for the

679 nm diode can offer satisfactory performance.

The free-running P-I curve is shown as black dots in figure 2.19. From specification, the typical operating current for the 707 nm (679 nm) diode is 75 mA (100 mA), corresponding to 50 mW (50 mW). Another clear feature is that the P-I curve of the ECDL is lower than the free-running P-I curve, which is expected as some output power from the diode is reflected back into the diode, and the optical isolator and fiber coupling will introduce loss.

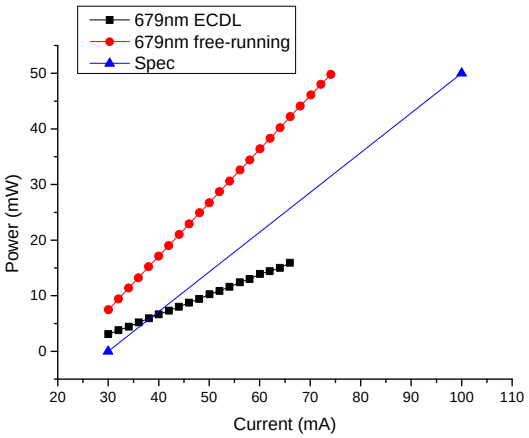


(a) λ-T curve for the 679 nm diode

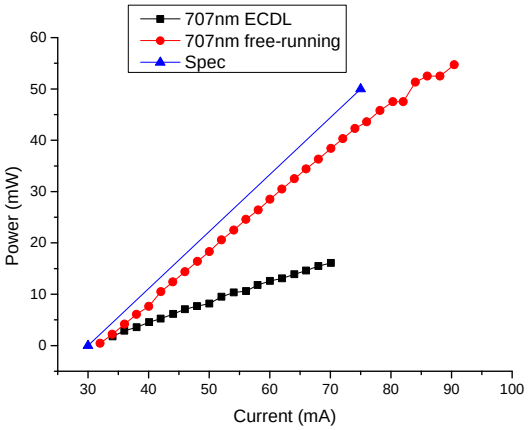


(b) λ-T for the 707 nm diode

Figure 2.18: Free-running λ-T curves for both diodes. The target wavelength for the 679 nm diode is lower than its free-running wavelength; the target wavelength for the 707 nm diode is higher than its free-running wavelength.



(a) P-I curves for the 679 nm diode

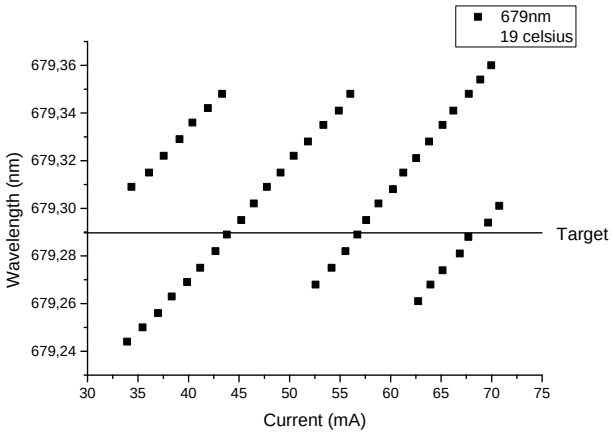


(b) P-I curves for the 707 nm diode

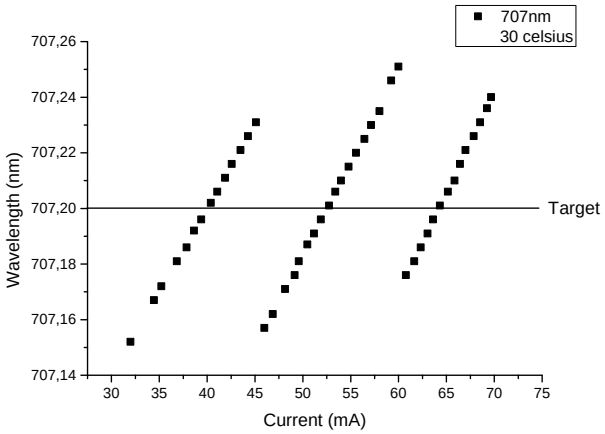
Figure 2.19: P-I curve for the free-running diode, the ECDL and the Spec.

2.3.2 ECDL Characterization

The main purpose of ECDL characterization is to check whether the grating is aligned properly to offer a good operation range. For each specific grating position, the λ-I curve features several parallel lines. The sudden drop is where mode-hopping occurs. For good alignment the target wavelength intersects the center of each parallel lines. The two final λ-I curves are illustrated in figure 2.20.



(a) λ vs. I curve for the 679 nm ECDL



(b) λ vs. I curve for the 707 nm ECDL

Figure 2.20: Final λ-I curves for both ECDLs. The temperature for each measurement is written in the figures.

Another important information from figure 2.20 is that only a finite number of electric current points can offer the right laser wavelength for a fixed temperature.

The ECDL's P-I curve is shown as the red data in figure 2.19. As the use of an external cavity increases the optical power buildup in the laser diode, degradation of the diode will inevitably be accelerated. So inspecting output power from an ECDL is important. This concern also suggests that the safest strategy is to operate the ECDL at a low current accompanied with a slave laser as power amplifier.

For the 679 nm and 707 nm diodes, the typical free-running operating current is 100 mA and 75 mA. We found that two months of 50 mA ECDL operation degraded both diodes significantly. We are now running the 679 nm ECDL at 38 mA, the 707 nm ECDL at 44 mA.

2.3.3 Short-term Linewidth

Characterization of the two ECDLs' linewidth is for the moment absent as they were urgently needed in the SrPAL project. However, a previously built 689 nm ECDL, which used an older-version grating mount and base (as in section 2.2), was characterized and documented in[15].

500 kHz linewidth was illustrated in this older-version ECDL. The measurement was done by beating that laser with a narrow-linewidth 689 kHz laser (2 kHz). During measurement, the ECDL was placed on a double-layer cushion, with polystyrene as the bottom layer and vibration-absorbing foam as the upper layer, with the temperature stabilized. The whole setup was placed on an optical table.

The linewidth of the two repump ECDLs built in this work are expected to be narrower than 500 kHz. Two repump ECDLs use the updated grating mount and base, which can provide better mechanical stability. Also, we built additional external housings made of polystyrene and vibration-absorbing foam to cover the huge bulk of the ECDL. So better thermal and acoustic decoupling can be achieved than in the previous linewidth measurement of the older-version ECDL.

2.4 Slave Laser Construction and Injection Locking

The 707 nm diode degraded due to long-hour high-current operation. So a slave laser was built and integrated into the final laser setup (chapter 3). This section describes our homemade slave laser's design and construction, followed by injection locking.

2.4.1 Construction of Homemade Slave Laser

Our slave laser design is simple and straightforward, consisting of a housing, a collimation tube, a copper mount, and a telescope (figure 2.21). As injection locking uses light from a master laser, which will be amplified in the slave laser's diode chip, no active feedback is required.

The aluminum housing features a massive pedestal at the bottom. A TEC is inserted between the copper base and the housing for temperature stabilization. The pedestal of the housing essentially acts as a heat sink.

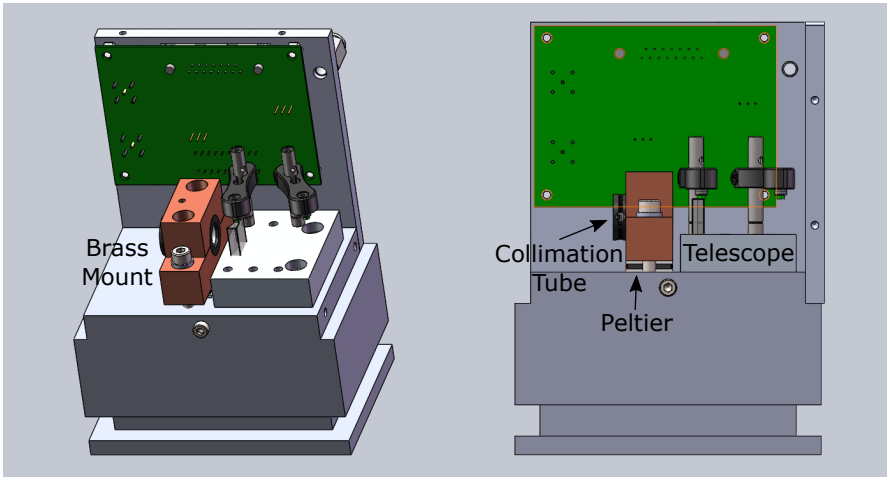


Figure 2.21: Homemade slave laser design.

The copper mount is bolted to the housing. The TEC stabilizes the temperature of both the collimation tube and the copper mount. As the heat sink should be thermally separated from the stabilized part, plastic washers are used in the bolt clearance holes. Additionally, two 2.5 mm holes are drilled in the copper mount to hold two NTC thermistors, one for PID error signal generation and the other for temperature readout.

The telescope is the same as in our ECDL design in section 2.2.

Slave Laser Assembly Procedures

Step 1

As in the ECDL assembly, the very first step is to collect everything needed. Commercial parts include a fully assembled collimation tube and the telescope

lenses, the same as in Tab 2.1. Homemade parts include a slave laser's housing, a copper mount, a telescope mount and various cables for electronics.

Step 2

The second step is to characterize the laser diode and test electronics. The electronics for temperature stabilization can be assembled and tested without the collimation tube plugged.

Step 3

The final step is to mount the collimation tube and the telescope. Before plugging the collimation tube in the copper mount, thermal paste must cover the tube for better thermal coupling between the tube and the copper mount. A practical detail is that the plugged tube should not stick out forward from the copper mount otherwise the telescope mount cannot fit in its designated position. The method to mount and align the telescope is the same as in section 2.2.

2.4.2 Injection Locking

The basic mechanism of injection locking is stimulated emission. Seeding light from an ECDL will retrace the slave's beam path back into the slave's diode chip. Because injection locking involves two counter-propagating beams, an optical isolator is essential for successful locking.

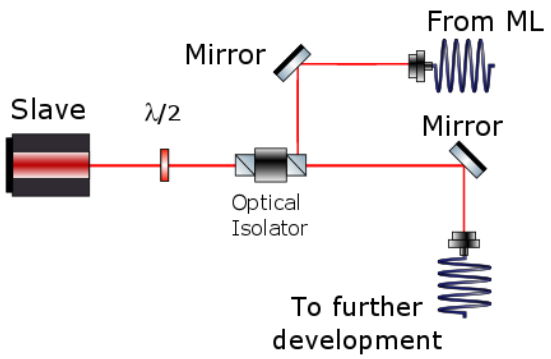


Figure 2.22: Schematic of basic injection locking geometry.

Injection locking requires one half-waveplate, one optical isolator, a polarization maintaining fiber, seeding light and enough degrees of freedom (figure 2.22).

Seeding light is sent into the side window of the second PBS in the optical isolator. By doing so, the seeding light happens to match the first PBS and will be coupled into the laser diode.

Procedures for Injection Locking

Step 1

The half-waveplate and the optical isolator can be placed directly in front of the slave laser. The side window of the second PBS must be rotated flat to the table, either facing left or right according to the designed optical setup.

Step 2

As a PBS is not a perfect polarization filter (particularly for the reflected light), leaking light will come out of the side window of the second PBS acting as a guide beam. The fiber collimator for the seeding light and a mirror can be placed as in figure 2.22 to couple the guide beam into the fiber. By doing so, when seeding light is injected from the other side of the fiber, it will retrace the guide beam and be coupled into the diode chip. The seeding light's polarization must match the second PBS for proper injection. In order to make the match, the fiber collimator can be rotated to change the direction of the seeding light's polarization, acting equivalently to a half-waveplate.

Step 3

A wavemeter and a scanning Fabry-Perot interferometer are used to monitor the slave's output and check whether injection locking is successful. Beforehand, the temperature of the slave should be set to the favoured level. Then, when the slave's operating current is turned on and tuned to single-mode operation condition, injection locking should be observed. When the slave is injection-locked, a clear single peak can be seen from the scanning Fabry-Perot interferometer, and the wavemeter ought to show the same wavelength as the master.

Chapter 3

ECDL Locking, Power Distribution and Repumping

Chapter 2 tells the story of building two ECDLs that can drive the $^3P_0$-$^3S_1$ and $^3P_2$-$^3S_1$ repumping transitions in ultracold strontium gas. The heavy and stable housing of the ECDL and the optical feedback from the grating together can significantly reduce the laser linewidth. However, mechanical and thermal perturbation from the environment still inevitably exist causing instability of the ECDL in both short-term and long-term.

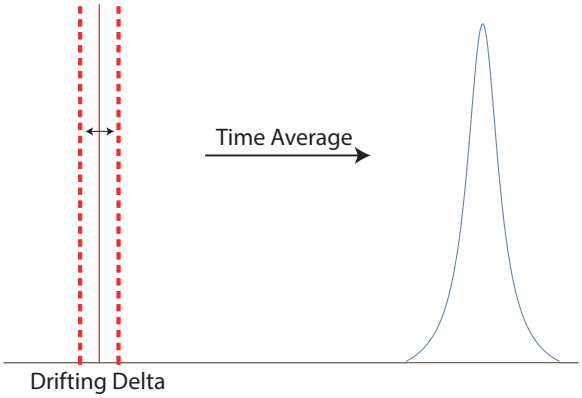


Figure 3.1: Laser instability. If the laser's frequency is not stable, the time average of such frequency domain motion exhibits a finite linewidth.

Short-term instability can be pictured by thinking of an oscillating single-frequency laser (figure 3.1, neglecting Schawlow–Townes linewidth). This frequency-

domain motion results from length changes of both the intra-cavity and the external cavity caused by environmental fluctuation. If this instability is averaged over a certain amount of time (normally µs or ms), a finite linewidth is obtained. Long-term instability is caused for the same reasons, but this frequency domain motion is much slower as the drifting of the laser's central frequency. For a mathematical model to explain laser instability, reference [23] is highly recommended.

As a result, although an ECDL possesses much better stability than a bare laser diode, proper thermal and mechanical decoupling from the environment must be achieved, as in our repump ECDLs. However, mere good passive stabilization still cannot offer sufficient stability for MHz or even kHz precision in controlling laser frequency, which is typically required in atomic physics. For instance, our older-version homemade ECDL exhibited a 500 kHz short-term linewidth but its central frequency drifted by 30 MHz per hour, even when temperature is stabilized. So active stabilization using a feedback loop with a very stable, definite frequency reference must be implemented. In conclusion, a laser must be stabilized, or "locked" to a reference such that both short- and/or long-term (which is more important in our case) stability can be realized.

Currently we lock both repump ECDLs to one homemade optical cavity (5200 finesse) using the Pound-Drever-Hall (PDH) technique. As an optical cavity is not an absolute reference, calibration of the cavity's length using the repumping signal from a strontium blue MOT is performed on a daily basis. In fact for the Sr repumping transitions, locking the two ECDLs to the respective transitions is more advantageous. The reason is that our repump ECDLs can offer sufficient stability (< 500 kHz) for the two MHz-linewidth repumping transitions, meaning that prevention of the long-term frequency drift is prior to reduction of the laser's linewidth through an optical cavity. However, building a spectroscopy cell for the two repumping transitions in strontium is difficult as the lower states are not the ground-state. The traditional heat-pipe scheme cannot provide sufficient population on the two initial states so the absorption signal is negligible. Indeed, electric discharge from a hollow-cathode lamp can effectively populate the two states, and this apparatus has already been implemented in many labs such as JILA [24] and MPQ [25]. Unfortunately, this device is so far absent in our lab. In contrast, we do have our own design of a high-finesse cavity. So eventually we

chose PDH locking calibrated manually through the repumping signal in the 2D blue MOT of the SrPAL machine.

3.1 Pound-Drever-Hall scheme

As the Pound-Drever-Hall technique is chosen as the locking scheme for the two repump ECDLs, this section is dedicated to its basics. Interested readers can refer to [26] for a thorough mathematical description.

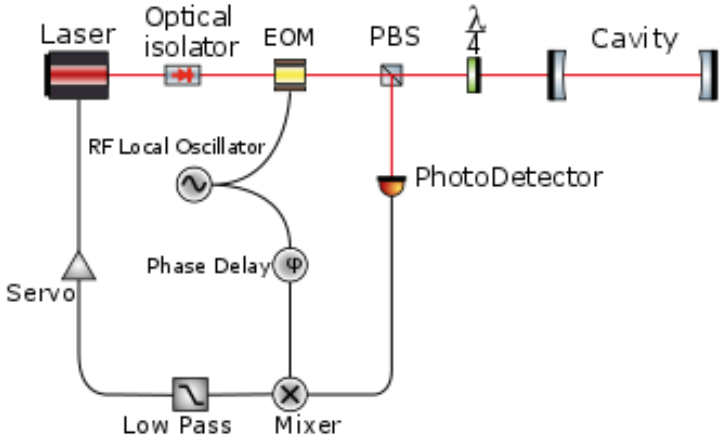


Figure 3.2: Schematic of basic PDH setup.

The PDH technique combines phase modulation of the laser beam, reflection from a cavity and electric demodulation to generate an error signal for closed-loop feedback [27]. Figure 3.2 depicts the basic geometry of the PDH setup. The locking position is one of the zero reflection points of the cavity, which is also the 100% transmission point (figure 3.3a). The process of the locking is dynamical. The job of the feedback is to apply deliberate "noise" to compensate environmental noise. As each feedback loop has a certain bandwidth, the laser frequency will still inevitably oscillate around the locking point. But still, a narrower laser linewidth can be realized than in the unlocked case.

The basic process of the PDH scheme is as follows. First, the laser is sent through a phase modulator, i.e. an electro-optic modulator (EOM) driven by a radio frequency (RF) oscillator. The RF is normally tens of MHz, much larger than

the cavity linewidth but much lower than the cavity's free spectral range ($\delta f \ll \Omega \ll \Delta f$, figure 3.3). The **phase-modulated** light is then coupled into a cavity. The reflected light from the cavity is collected by a photodetector (PD). The raw PD signal is **encoded with the error signal**. Next comes the "decoding" process (demodulation). The PD raw signal and the very same RF signal applied on the EOM are "mixed" by a mixer. A phase delay is always needed to match the phase of two signals in order to extract the correct and the optimized component. Then the signal is sent through a proper low-pass filter to extract the final **demodulated** error signal, which tells the servo how to correct the laser frequency once it deviates from the locking point.

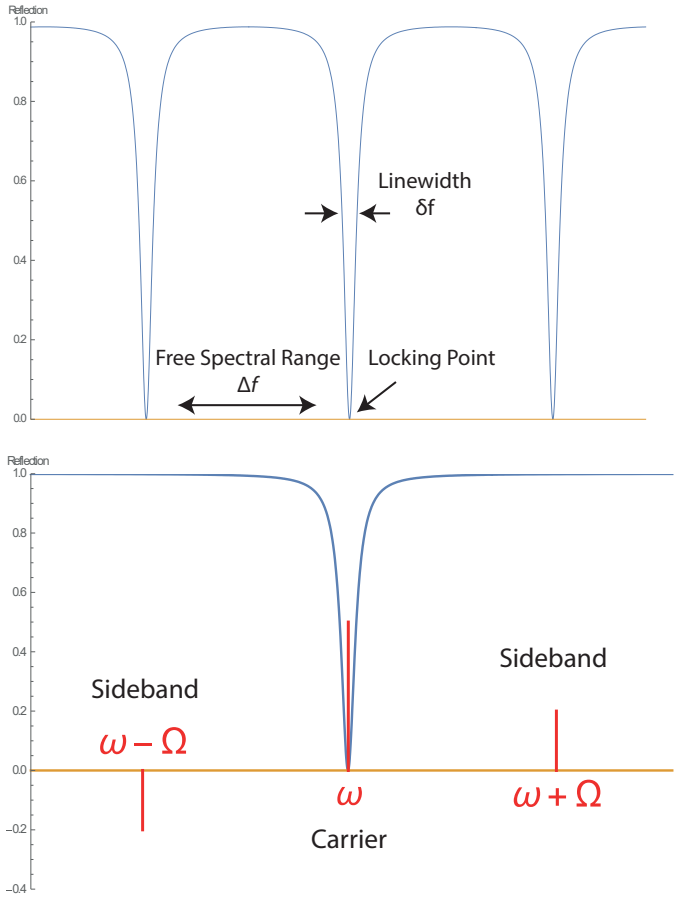


Figure 3.3: Top: a cavity's reflection profile. Bottom: the relative positions of a carrier and two sidebands with respect to the locking position.

According to the derivation in [26], a typical PDH error signal is depicted in figure 3.4. The central part of the error signal is a linear locking region where a "restoring force" is offered. However, the error signal does not reverse sign till the sideband frequency points. So the locking region may extend to the corresponding two zeros. In fact, the maximal locking region is limited within the two local minimums as bounded by the black-dashed lines in figure 3.4. The area bounded by the red-dashed lines denotes a typical locking region. A various factors can affect the locking performance including bandwidth of the feedback loop, choice of the modulation frequency and the cavity's parameters (FSR, finesse, linewidth) etc.

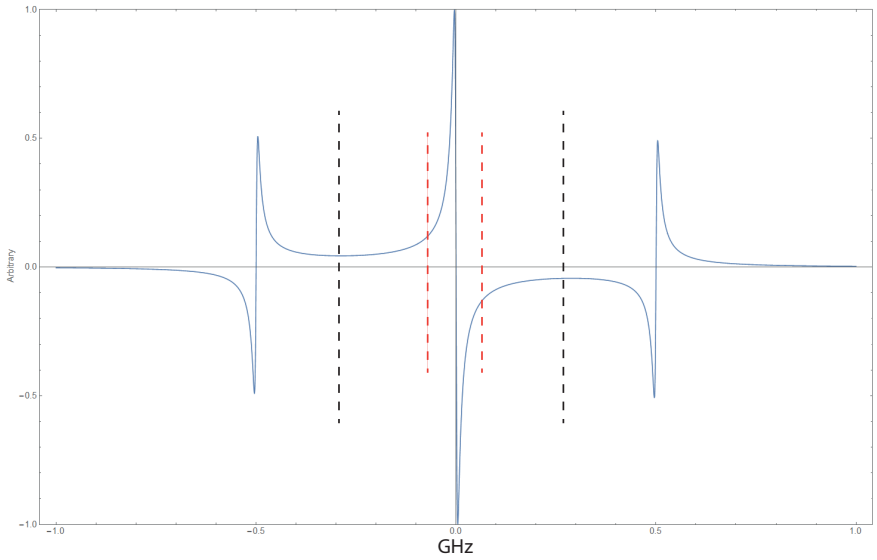


Figure 3.4: A PDH error signal. FSR is 1 GHz, modulation frequency is 500 MHz, finesse is 1500.

3.2 Repump Laser Setup

A schematic of the repump laser setup is depicted in figure 3.5. Optical power is finally distributed into three paths to the SrPAL machine, one for Sr 2D blue MOT and two for Sr red MOT. Cavity-locking, and injection-locking for the 707 nm slave both require a small portion of optical power. So most of the optical power is either sent into the machine or lost.

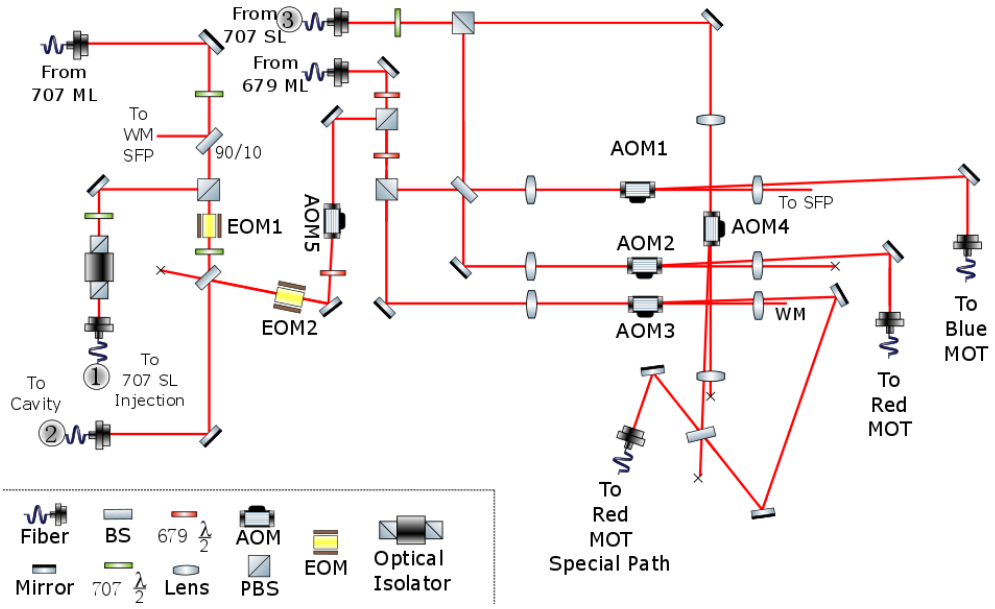


Figure 3.5: Schematic of the repump laser setup, consisting of the PDH modulation path and three paths towards the SrPAL vacuum chamber. "SL" stands for slave laser; ML stands for master laser.

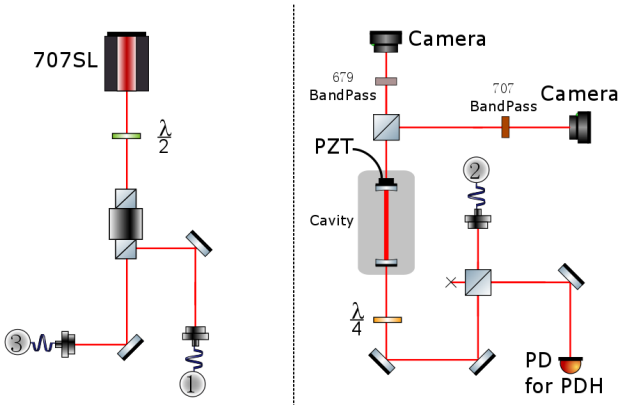


Figure 3.6: Left: The 707 nm injection-locking path. Right: the cavity-locking path.

We are now running the 679 nm ECDL at 38 mA to obtain 6 mW output power and the 707 nm ECDL at 44 mA for 2 mW power. Power from the 679 nm ECDL is sufficient to distribute in both the cavity-locking path and experiment paths; The diode in the 707 nm ECDL degraded and this ECDL's output is just enough for the cavity-locking and injection-locking, so a slave laser is used for power amplification. Finally, 80 µW optical power from each ECDL is sent onto the cavity for PDH locking; 500 µW from the 707 nm ECDL goes into the slave; each of the three "to experiment" beams contains 600 µW from each ECDL. Despite this looking quite small, it is already enough to saturate repumping in the SrPAL machine.

3.2.1 PDH Cavity Locking

The locking cavity for the repump ECDLs has 1.5 GHz free spectral range, 5200 finesse (99.94% reflectivity for both mirrors) and thus 300 kHz linewidth. This cavity was designed and made by previous team members, and is well documented in [28].

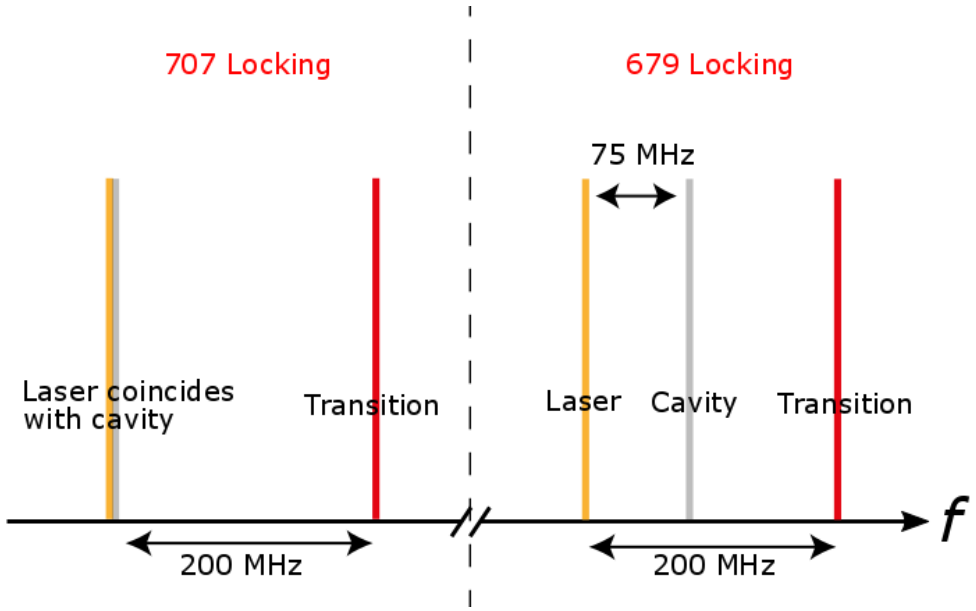


Figure 3.7: Locking scheme for the repump ECDLs. Two lasers are locked to two different resonance peaks of the same cavity.

As we lock two lasers on the same cavity, the two locking points are not likely to coincide with the two transitions simultaneously. So a frequency gap must be bridged and we finally designed a locking scheme.

The locking scheme is depicted in figure 3.7. The cavity must be calibrated first for the designed locking configuration. Our cavity is assumed to drift 10 MHz/day if properly isolated, so the calibration is performed on a daily basis. Both 707 nm and 679 nm ECDLs are locked 200 MHz red to the respective transitions, as 200 MHz up-shifted AOMs are used as fast switches for experiments.

Two different modulation frequencies and two sets of electronics are used. The modulation frequency is $\Omega_1 = 14.89\,\text{MHz}$ for the 679 nm ECDL, and $\Omega_2 = 22.9\,\text{MHz}$ for the 707 nm ECDL. Coexistence of the two modulation frequency will introduce an additional frequency component in the demodulated error signal ($\Omega_2 - \Omega_1 = 8.01\,\text{MHz}$), so we use single-pole low-pass filters with 500 kHz cutoff frequency for both feedback loops. In order to monitor the cavity's transmission light to indicate the locking points, two optical bandpass filters and cameras are used. Figure 3.8 shows the two clear TEM_{00} modes when both ECDLs are locked. However, a problem arises as two beams go through the same quarter waveplate in the cavity-locking path (figure 3.6). This particular quarter-waveplate is customized for 679 nm light. We found that when polarization of the 679 nm light was transformed from linear to circular, polarization of the 707 nm light is very close to perfect circular but cannot reach it. We also tried other quarter-waveplates but the result was even worse. Luckily, this imperfection does not degrade the error signal (figure 3.9) and we can still lock both ECDLs simultaneously.

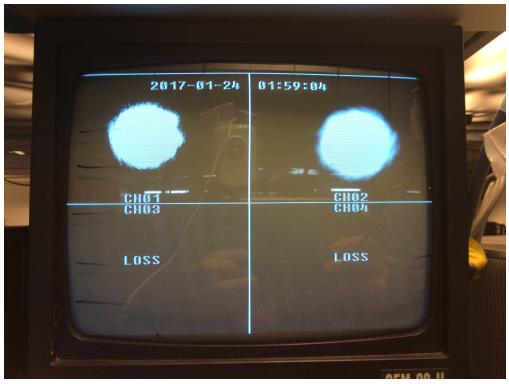


Figure 3.8: Two TEM_{00} modes indicating that both ECDLs are locked.

A feature of the electronics used for PDH locking is that they are all homemade. The PI controller for the feedback loop is inherited from prof. Walraven, which is homemade and sadly both P and I gains can only be tuned by re-soldering new resistors and capacitors. Currently, feedback signal is applied to both PZT and electric current. The DDS and the associated power amplifiers were designed by Florian Schreck and collaborators [13].

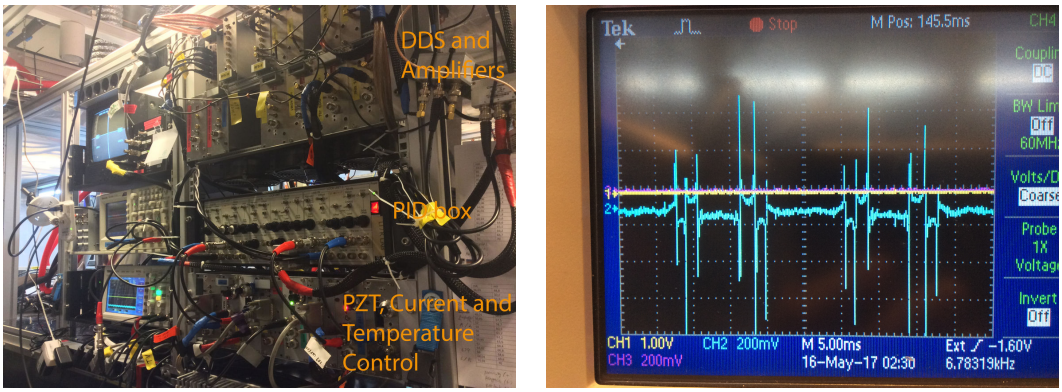


Figure 3.9: Electronics used in the repump laser setup, and the error signal from an oscilloscope when the ECDL's PZT is scanned.

3.2.2 Beampaths to the SrPAL Machine

The two ECDLs' optical power is finally distributed into three paths for experiments: blue MOT path; red MOT path; red MOT path along with transparency beam. This laser setup is built for the SrPAL project, and each path has its own specific function, which will be explained below.

Blue MOT Path

This path is labeled the "To Blue MOT" in figure 3.5. Light of this path directly impinges on the Sr 2D blue MOT and continuously repumps atoms in the ${}^3P_0$ and ${}^3P_2$ metastable states. The atomic density in the blue MOT is increased so that more atoms can be transferred from the 2D blue MOT to the lower-positioned red MOT. Laser beams from two ECDLs go through the same 200 MHz up-shifted AOM before being coupled into the same fiber. Before entering the blue MOT chamber, the two-color light from the fiber is expanded to 5 cm diameter to cover as much area of the 2D blue MOT as possible.

Red MOT Path

This path is labeled "To Red MOT" in figure 3.5. Light of this path covers as much region of the red MOT as possible. The purpose of this path is to repump metastable atoms before making absorption images. The fiber output is expanded to 1 cm diameter before going into the red MOT chamber. The same as above, a 200 MHz up-shifted AOM (AOM2) is used.

Red MOT Path with Transparency Beam

This path is labeled "To Red MOT special path" in figure 3.5. repump light in this path continuously repumps metastable atoms in the red MOT, which are produced by a "transparency beam".

The cooling transition of a Sr red MOT is closed, so normally a Sr red MOT does not require any repump laser. The reason to set up this path for SrPAL is as follows. SrPAL machine aims to produce a perpetual Sr BEC using the red MOT as a reservoir to continuously replenish the final out-coupled atom laser. But any near-resonant light will destroy the BEC. Currently, the solution is to use a laser largely detuned from $^3P_1$-$^3S_1$ transition in order to shift the $^3P_1$ state. Thus, the cooling light of the red MOT becomes transparent to the energy-shifted atoms. Though this laser is several GHz detuned from the resonance, some Sr atoms in the red MOT are still pumped to the $^3S_1$ state and finally reside in the two metastable states. This accidentally induced loss destroys the red MOT in SrPAL. Two repump lasers are thus needed.

In this path, two repump lasers and the transparency beam are coupled into the same fiber, so they can address the same atoms in the red MOT. In contrast to the above two paths, the two repump laser beams pass separate AOMs for independent frequency control.

3.3 Theoretical Aspects of Repumping Effect in Strontium

The necessity of repump lasers in any MOT directly arises from the MOT's imperfect operation. This section is dedicated to the theoretical aspects of MOT and repumping in strontium.

3.3.1 Strontium Blue MOT and Repumping

The Sr cooling scheme was pioneered by Katori *et al.* using a two-stage MOT sequence. The first stage MOT operates on the $^1S_0$-$^1P_1$ transition, which is strongly electric dipole allowed resulting in a 30 MHz transition linewidth. The corresponding strong scattering rate can provide a large cooling effect. But accordingly its saturation intensity and the Doppler limit is high [13]. For simplicity, the following discussion does not include the hyperfine structure of ^{87}Sr and is only restricted to the bosonic isotopes.

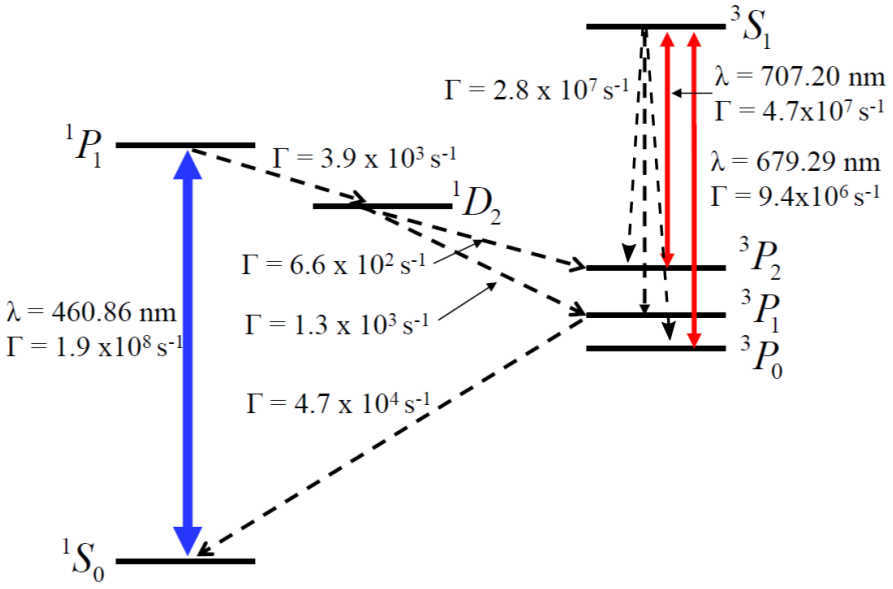


Figure 3.10: Relevant energy levels for repumping Sr atoms. ***Adapted from [7].***

The blue MOT cycling is almost closed, having a tiny leakage. Indeed most of the $^1P_1$ atoms will decay to the ground state, but a very small fraction will first decay to the intermediate $^1D_2$ state followed by 1/3 of them leaking to the $^3P_2$ metastable state and 2/3 to the $^3P_1$ state. The lifetime of an atom in the $^3P_1$ state is 20 µs. So atoms leaking to this state will rapidly go back to the ground state while they may still stay within the capture range of the blue MOT. But the channel to the metastable $^3P_2$ state is troublesome. Luckily, the branching ratio to the intermediate $^1D_2$ state is so small (1:50000 in ^{84}Sr [10]) that a Sr blue MOT can still be produced by mere blue cooling lasers. However, when a large

atom number is needed, repump lasers become important. This leaking channel, interestingly, can efficiently populate the $^3P_2$ state, which happens to be trapped in the quadrupole magnetic field of a blue MOT. This serendipity was essential in the creation of the first strontium BEC [10].

Two repumping schemes are commonly used in Sr. The first is through driving the $^3P_2$-$^3D_1$ ($5snd$) transition. The advantage of this repumping scheme is that only one laser is required [29]. However, the frequency of this transition is not conveniently accessible with current laser diodes. The second scheme is used in this thesis work: repumping through the $^3S_1$ state with two repump lasers. Initially, only the $^3P_2$ state is populated from the loss in a blue MOT. By applying a 707 nm laser ($^3P_2$-$^3S_1$), $^3P_2$ atoms will be pumped to the $^3S_1$ state and $^3S_1$ atoms will decay to all ^3P_J triplet states (figure 3.10). Newly populated $^3P_2$ atoms will again be repumped; but newly populated $^3P_0$ atoms will be lost. Therefore, a 679 nm laser ($^3P_0$-$^3S_1$) is needed to deplete the $^3P_0$ population. This scheme's advantage is the accessibility of relevant laser diodes and their cheap price. But using two lasers is relatively less convenient.

3.3.2 SrPAL Red MOT and Repumping

The second stage MOT in Sr operates on the $^1S_0$-$^3P_1$ transition (689 nm), which is spin-forbidden rendering a 7.4-kHz linewidth, much narrower than common cooling transitions, which typically are several MHz wide. This narrow linewidth enables cooling down to the recoil temperature limit [9].

This MOT cycle is closed, so normally no repumping is needed. As introduced in chapter 1, the main goal of the SrPAL project is to build the first perpetual atom laser, which is based on the pioneering work in [12]. In the SrPAL project, a BEC has to be created inside the red MOT. As any near-resonant photon will heat the BEC and destroy it, a "transparency" laser, which is largely detuned (GHz) from the $^3P_1$-$^3S_1$ resonance in Sr, is used to induce an AC-Stark shift on the $^3P_1$ state so that the Sr atoms become transparent to the red cooling photons. Though this laser is far away from the transition, it may still pump atoms to the $^3S_1$ state and thus populate the two metastable states. In the SrPAL machine this additional loss destroyed the red MOT. In order to restore the red MOT, the 679 nm and

707 nm repump lasers are needed to continuously deplete the population in the two metastable states.

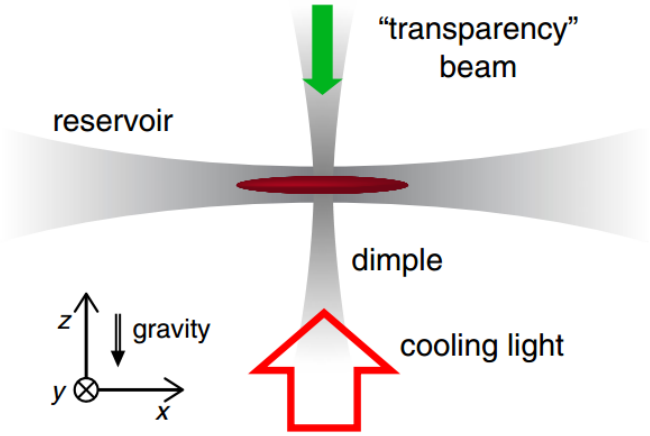


Figure 3.11: The pioneering work of making a BEC only through laser cooling. In the SrPAL machine, a different geometry is used but the transparency beam remains. ***Copied from [12].***

3.4 Characterization of Repumping and Frequency Measurement of the Two Repumping Transitions

We characterized the repumping in the SrPAL machine, and roughly measured the two repumping transitions. As the SrPAL project aims to build an atom laser of ^{84}Sr, the following results are only valid for this particular isotope.

3.4.1 Characterization of Repumping

The most direct phenomenon induced by repumping is fluorescence blinking in a MOT when the frequencies of repump lasers are scanned and cross the transitions, because the fluorescence will be increased when the repump lasers are on resonance. Figure 3.12 shows the recorded fluorescence images in both-off, 707-only, and both-on cases. The fake color is dependent on the atomic density, e.g. the central red part is denser than the peripheral area. The difference in the fluorescence between

the both-on and the only-707 cases is not very sharp (but still distinguishable), while the only-707 case is clearly different from both-off case.

The fluorescence vs. power curve is measured for the two lasers (figure figure 3.13 and figure 3.14. Both beams are expanded to 5 cm diameter before entering the 2D blue MOT chamber. From the figures, 0.03 mW/cm^2 intensity from the 707 nm laser is needed to saturate the repumping signal. When the fluorescence is optimized using only the 707 nm laser, it can be further increased employing the 679 nm laser and only 0.003 mW/cm^2 intensity is required from it to saturate the repumping signal. The maximal fluorescence increase of the continuous 2D blue MOT of SrPAL is estimated to be 40%.

Table 3.1: Optical intensity to saturate the repumping signal in the blue MOT of the SrPAL.

	$^3P_0$-$^3S_1$ 679 nm	$^3P_2$-$^3S_1$ 707 nm
Intensity for Saturation	0.003 mW/cm^2	0.03 mW/cm^2

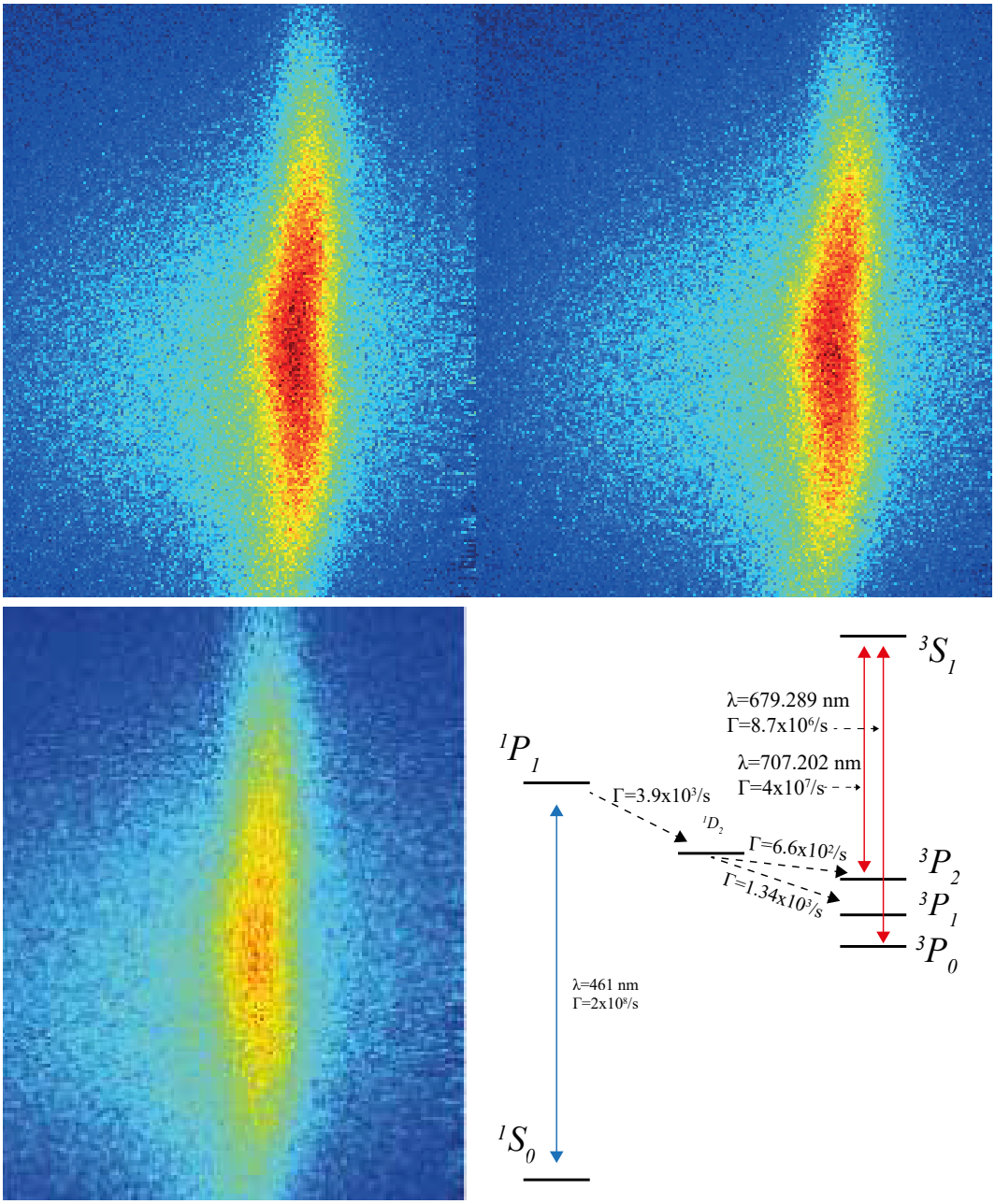


Figure 3.12: The repumping signal from the blue MOT of the SrPAL. Both repump lasers were set to the respective transitions and provide sufficient power to saturate the repumping signal. Top Left: When both repump lasers on. Top Right: When only 707 nm laser on. Bottom Left: When both repump lasers off. Bottom Right: The related energy levels for repumping.

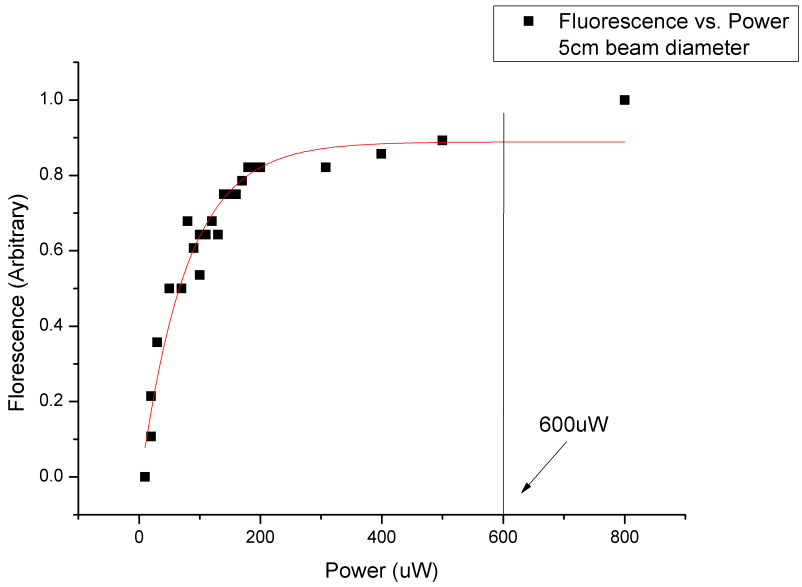


Figure 3.13: Curve of fluorescence vs. the optical power incident on the MOT from the 707 nm laser.

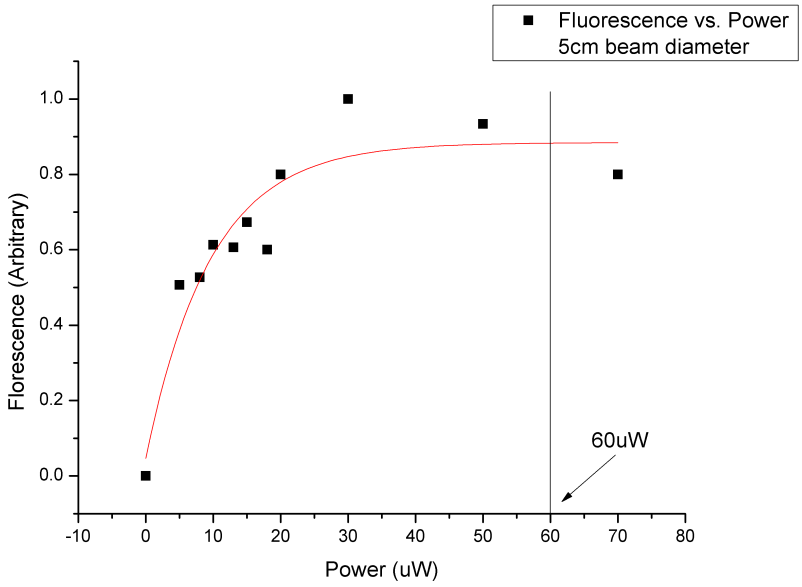


Figure 3.14: Curve of fluorescence vs. the optical power incident on the MOT from the 679 nm laser. Before the measurement, the 707 nm laser frequency was set to its repumping transition.

3.4.2 Measurement of the Two Repumping Transitions

With both the 679 nm and the 707 nm lasers at hand, a rough measurement of the $^3P_0$-$^3S_1$ (679 nm) and $^3P_2$-$^3S_1$ (707 nm) transitions can be carried out by scanning the PZTs while monitoring the readout of a WS7-30 wavemeter. The interest originates from that to our best knowledge, the two transitions have not been measured in ^{84}Sr (but the $^3P_0$-$^3S_1$ transition was measured in ^{87}Sr and ^{88}Sr [30]).

Measurement Method

Our measurement strategy is described in the following using the 707 nm transition measurement as an example (figure 3.15). We aligned the unlocked 707 nm laser onto the Sr blue MOT of the SrPAL, scanned the frequency crossing the transition and monitored both the frequency readout of the wavemeter and the fluorescence simultaneously in real-time. Figure 3.15 depicts the raw data obtained: the laser's frequency vs. time curve from the wavemeter, and the fluorescence vs. time curve from the fluorescence monitor. The saw-tooth shape in the bottom graph implies the frequency scan is quite linear with respect to time.

With raw data at hand, the task is to locate the transition points in the frequency vs. time curve. As each turning point in this frequency scan corresponds to a mirror-symmetric axis in the fluorescence vs. time curve, we can use such correspondence as reference to locate the transition points by calculating the spacings and the ratio. In figure 3.15, black lines denote the reference points and colored lines denote transition positions. By reading the "frequency ruler" (y-axis of the frequency vs. time curve), the transition frequency can be determined directly. The key of this strategy is to find the correct correspondence. As we obtained the both curves simultaneously, the last correspondence is clear and can be distinguished from the others.

The wavemeter (WS7-30), which can provide 30 MHz absolute accuracy[1] belongs to our neighboring Atom-Ion group of Rene Gerritsma. The wavemeter is currently calibrated on the narrow-linewidth (2 kHz) 689 nm laser from our lab, which is sent through a 50 m fiber connecting the two labs. Another 50 m fiber is plugged into the wavemeter with the other side in our lab so that we can send any laser beam of which we would like to know the frequency through the fiber.

[1] According to the 3σ criteria in the specification.

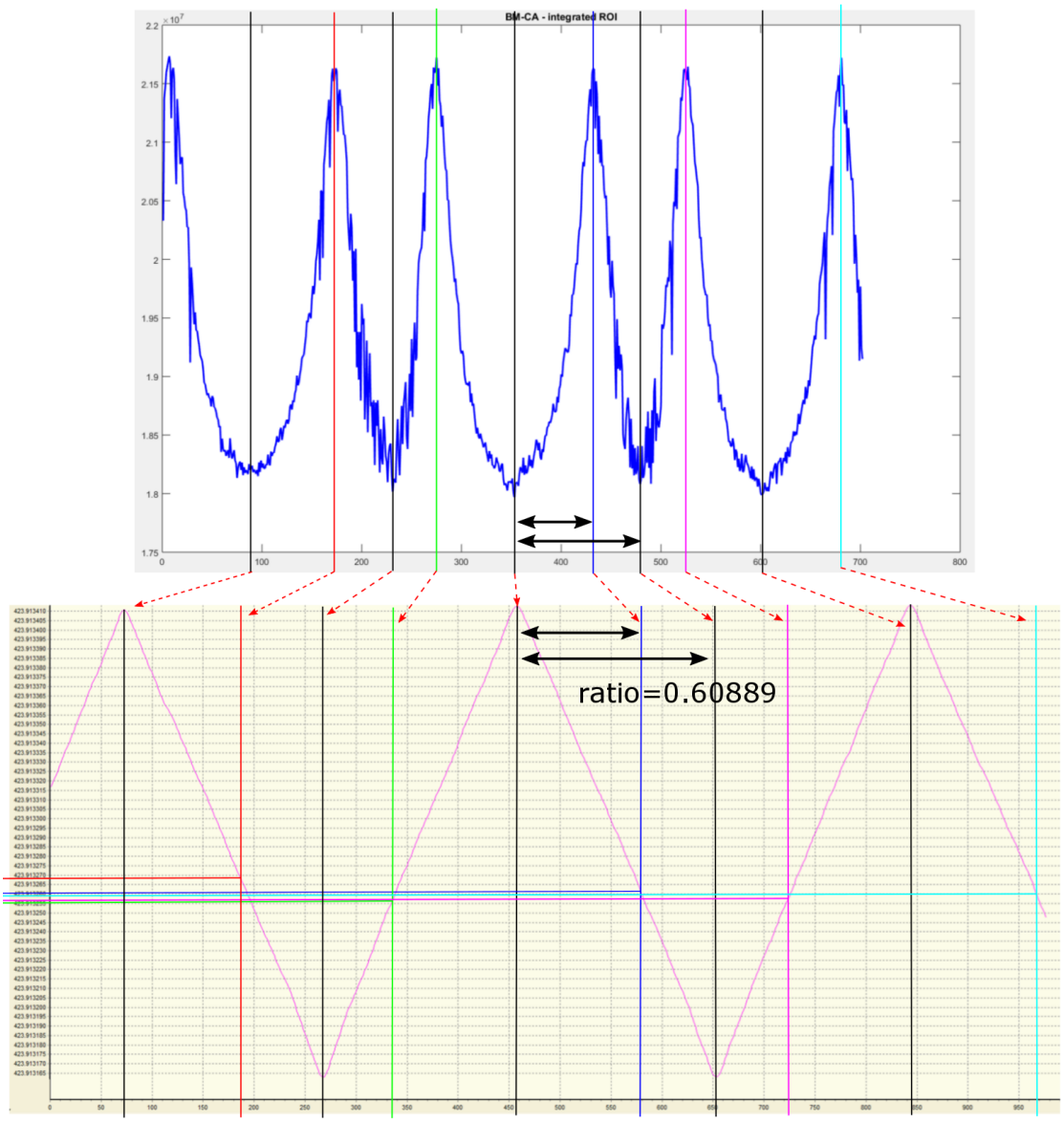


Figure 3.15: Data of the $^3P_2$-$^3S_1$ transition measurement. The measurement strategy is explained in the text. Here we actually measured the laser frequency, which was extracted before the laser went through a 200 MHz up-shifted AOM. From the bottom graph, five resonance points indicated by the colored lines can be located and are used in data analysis. In the $^3P_0$-$^3S_1$ transition measurement, seven such points in the frequency scan of the 679 nm laser can be located and used in the data analysis.

Result

As explained in section 3.2, each laser will go through an up-shifted 200 MHz AOM before impinging on the blue MOT. Beams from both characterized lasers were extracted before going through the AOM. So each transition frequency is the measured laser frequency plus a 200 MHz shift. The 679 nm transition was also measured and analyzed using the same method as explained above.

In the $^3P_2$-$^3S_1$ measurement we used a frequency ruler with 5 MHz-spaced markers, while in the $^3P_0$-$^3S_1$ measurement we used a frequency ruler with 1 MHz-spaced markers. This difference affects the final statistical uncertainty. Data and the final result are shown in table 3.2.

In the final result, only 30 MHz systematic uncertainty, i.e. the absolute accuracy of the wavemeter, is adopted. In the measurement, systematic errors include the wavemeter error (30 MHz), Zeeman shift (several MHz by estimation), blackbody radiation (negligible), light shift from the probe laser[2], etc. The 30 MHz uncertainty is so huge that other systematic errors will be submerged under this giant value so only the 30 MHz uncertainty is given in table 3.2. But as our measurement method is simple and rough, a larger systematic uncertainty is expected. The statistical uncertainty contains the standard deviation of each data set, and the respective reading error, i.e. 2.5 MHz for the 707 nm laser measurement and 0.5 MHz for the 679 nm laser measurement.

Table 3.2: The final result of the measurement.

Transition	Frequency (MHz)	Systematic Uncertainty (MHz)	Statistical Uncertainty (MHz)
$^3P_2$-$^3S_1$	423913460	30	6
$^3P_0$-$^3S_1$	441332834	30	3

[2]As the probe power is so tiny that this term is negligible.

Chapter 4

Iodine Spectroscopy As Absolute Reference

4.1 Introduction

Iodine molecule vapor can offer more than 100000 ro-vibrational transition lines in the visible and near-infrared region [31]. Each ro-vibrational line has hyperfine structure due to the hyperfine interaction induced by the large nuclear quadrupole moment of the iodine atom. Most of the hyperfine transition lines, with up to 1 GHz splitting, are easily resolved by saturated absorption spectroscopy. With such an abundance of transitions in a large frequency range, molecular iodine has been studied in many physical branches including precision measurement [32], optical clock [33] and laser modulation technology [34]. Also, molecular iodine spectroscopy can serve as a cheap absolute frequency reference for many transitions of interest provided the relevant iodine lines are well studied and identified, while a commercial wavemeter with very high precision and accuracy (MHz) is extremely expensive. For instance, one of the hyperfine transitions of R(37) 16-1 line at 578 nm can act as frequency reference for the Yb $^1S_0$-$^3P_0$ clock transition [35]; hyperfine lines near 548 nm can offer good reference for lithium ion spectroscopy [36].

In our lab, one ongoing project is to build a clock laser system to drive the $^1S_0$-$^3P_2$ transition (671 nm) in ^{87}Sr. The $^3P_2$ state in alkaline atoms is metastable as the $^1S_0$-$^3P_2$ transition is both electric dipole forbidden and spin forbidden. The

measured lifetime of the $^3P_2$ state in ^{88}Sr (boson) is 520 s [8] (mHz linewidth). In ^{87}Sr (fermion), similar to its $^3P_0$ clock state, hyperfine mixing [37] may still occur, rendering electric dipole transition very weakly allowed. In addition, by applying a small static magnetic field [38], a small fraction of the $^3P_1$ state can be mixed into the $^3P_2$ state, further broadening this transition. But still, sub-Hz transition linewidth is expected and accordingly a Hz-level stability is required for the laser.

When it comes to an ultra-narrow transition, a practical issue is to find a robust way to relocate the resonance as the transition linewidth is so narrow that the resonance signal is easily lost due to long-term cavity drift. Due to its abundance, versatility and also a precedent [35], it is decided to implement an iodine spectroscopy with the hope to make it a general reference for not only the clock laser, but also other lasers in our lab.

The typical pump-probe geometry was utilized and established. A previously home-made 688 nm ECDL, which can drive the $^3P_1$-$^3S_1$ transition of Sr, is used for the optical alignment and preliminary test of the iodine spectroscopy.

4.2 Saturated Absorption Spectroscopy

The simplest spectroscopy geometry is to use just one weak probe beam and measure its intensity reduction after going through the spectroscopy cell. By scanning this beam's frequency, a Doppler broadened signal will appear if background noise is cancelled. However, the natural linewidth of the transition is usually much shorter than this broadened one. The origin of this Doppler broadening is the thermal velocity spread as described by the Maxwell distribution, and the Doppler effect. The atomic velocity distribution in thermal equilibrium is the Maxwell distribution which is a Gaussian. An atom moving at velocity v sees a frequency-shifted probe beam according to the Doppler effect. Taking the two aspects into account, theoretical analysis illustrates a profile with much larger broadened linewidth. Depending on the temperature, this broadened linewidth can even reach GHz level. For instance, the natural linewidh of the $^1S_0$-$^1P_1$ transi-

tion in Sr is 30 MHz while its Doppler broadened linewidth is 860 MHz at 300 K[1].

However, a phenomenon can help to manifest the sub-Doppler profile, which is transition saturation. In a two-level system, a laser can drive the transition and thus re-distribute population in both states. In the steady state, population in the upper state saturates to $N/2$ with increasing optical intensity and decreasing detuning, where N is the total number of atoms [40]. As a result, when the transition is saturated using a strong "pump" beam (figure 4.1), absorption of the probe photons will be significantly suppressed. But as two beams travel opposite directions, they cause opposite Doppler shift for the same atom. Only when both beams address the same atom, absorption of the probe from those atoms will be reduced burning a hole in the Doppler broadened absorption profile (figure 4.2), i.e. the "Lamb dip".

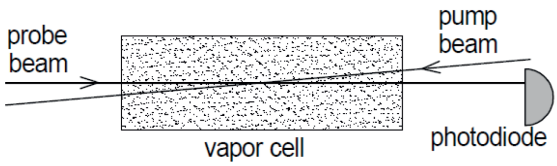


Figure 4.1: Pump-probe geometry. ***Copied from [39].***

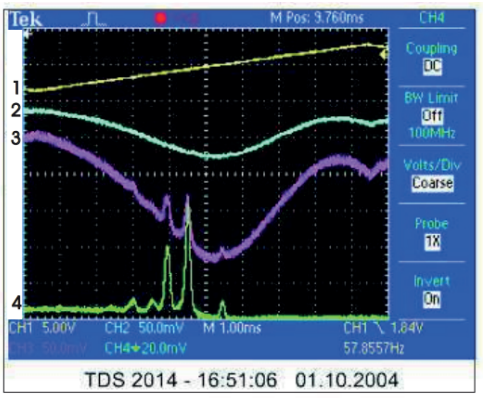


Figure 4.2: An example of the saturated absorption spectroscopy signals. (1)(2) are reference signals for background cancellation. (3) is the probe signal with Doppler broadened background and sub-Doppler dips. (4) is the differential signal between (3) and (2). ***Copied from [41].***

[1]the Doppler linewidth is given by $\Delta f = f_0\sqrt{\frac{8k_BT\ln 2}{mc^2}}$ where f_0 is the resonance frequency [39].

4.3 Experimental Setup

The building elements of this spectroscopy setup include a homemade iodine cell, electronics and an optical setup.

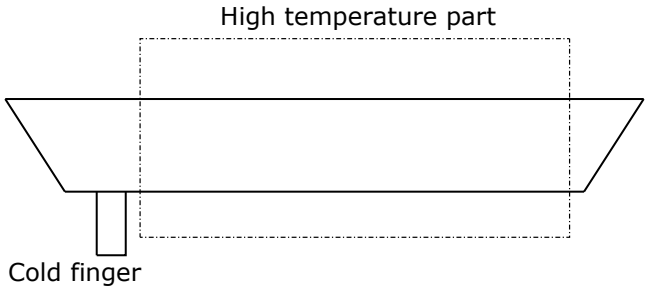


Figure 4.3: The cold finger and the heated part.

The working principle of the iodine cell is as follows (figure 4.3). The cell is sealed and filled with molecular iodine vapor. When the vapor and its condensate coexist in a closed environment, vapor pressure is determined by the temperature of the condensate. In this iodine cell, vapor pressure is controlled by controlling the temperature of a cold finger through a TEC. In the region away from the cold finger, the iodine vapor is heated up. Transitions of interest are normally between high lying vibrational states of the molecular ground-state potential and vibrational states in electronically excited potentials. So heating is required to populate enough molecules in the initial higher vibrational states. In our case, we are interested in transitions near 679.289 nm, 707.202 nm, 671.206 nm. From a commercial iodine spectrum calculator, useful lines may appear at 400 °C or even higher temperature. So our target temperature is 500 °C.

The real iodine cell is shown in figure 4.4. The glass cell is embedded in an aluminum housing filled with thermal insulating stuffing. The cell is heated by a resistive heater, up to 600 °C according to previous users. A water cooling element is inserted inside to cool down electronics and other elements which should not be heated up. The cooling water also cools down the heat sink for TEC. The heater was driven by a variac. However, it was found that the temperature could

not climb higher than 250 °C. So it was decided to cover the housing with foil as shown in figure 4.4. However, low temperature plastic insulated cables inside the cell were shortened and caused power outages. We are in the process of replacing the plastic insulated cables by glass fiber insulated high temperature cables, which should allow us to reach 500 °C in the near future.

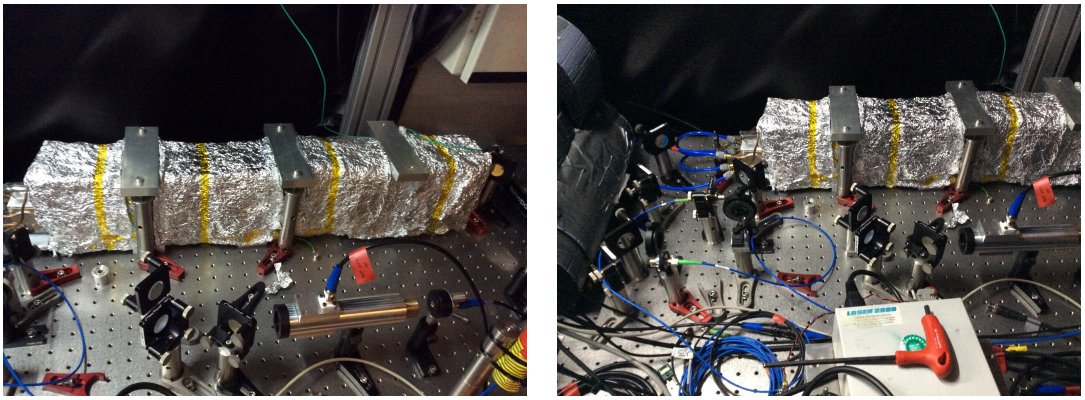


Figure 4.4: The real iodine cell covered with aluminum foil.

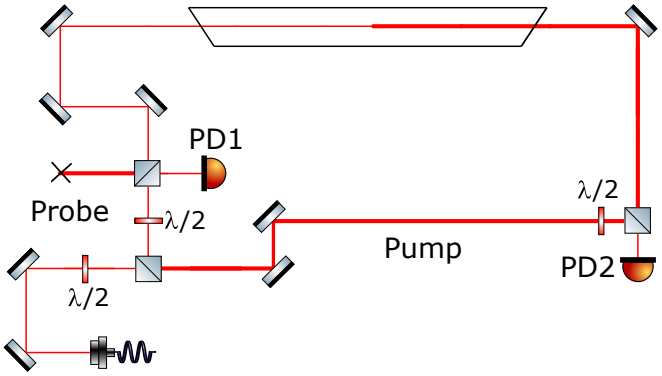


Figure 4.5: Schematic of our iodine spectroscopy setup.

Although there are problems with the cell, the optical setup is finished except newly conceived telescopes. Figure 4.5 depicts the schematic of the optical setup. The use of extra mirrors is due to spatial constraint on the optical table. The standard pump-probe geometry is used for the setup. On the probe path, a reference beam is extracted for background noise cancellation. On the pump path, enough space is spared to insert an EOM or AOM in the future.

The alignment of optics was performed using an available homemade 688 nm ECDL. Before the electronic shorting when temperature could at most climb 250 °C (without foil), a preliminary test was performed. Near 687.993 nm, a weak absorption signal was observed. The peak-to-peak depth was 20 mV while the background offset was 250 mV. Probe and pump power were 80 µW and 2 mW respectively. The fiber beam was collimated by a 7.5 mm collimator resulting in a 2 mm beam diameter. The corresponding intensities were 2 mW/cm^2 and 60 mW/cm^2 for the probe and pump respectively. The intensity on the probe path might be too high because the probe intensity is normally a fraction of the transition's saturation intensity (100 µW/cm^2 for a typical MHz linewidth transition). Both beams should be expanded to fill the optical entrance's full cross-section. So telescopes are required which can be implemented in the future.

Two possible reasons may account for the weak absorption signal. First, the huge pump intensity saturates the transition so much that the probe light can only be weakly absorbed. Implementing telescopes may solve this problem. Second, the weak signal may result from low population in the initial state (too low cell temperature) and low vapor pressure which limits the number of interacting atoms (too low cold finger temperature). So higher temperature for both cell and cold finger may help.

Chapter 5

Summary and Outlook

5.1 Summary

This thesis describes three pieces of work.

The first onn (chapter 2) is the construction of two homemade External Cavity Diode Lasers (ECDL) and a slave laser to drive the $^3P_0$-$^3S_1$ and the $^3P_2$-$^3S_1$ transitions in ultracold strontium gas. Design and detailed construction procedures for the ECDLs are described, and we hope this chapter can become a good reference guide for building similar ECDLs and slave lasers. The two ECDLs were characterized, focused on the optical power, temperature and lasing wavelength, all of which determined the reasonable operation condition for each ECDL.

The second main work (chapter 3) is locking two ECDLs to a high-finesse cavity using the Pound-Drever-Hall technique, distributing the optical power, and performing experiments related to the repumping of strontium in the Strontium Perpetual Atom Laser (SrPAL) machine. As an optical cavity is not an absolute frequency reference, the 2D blue MOT of the SrPAL is used for frequency calibration. By shining two lasers on the 2D blue MOT and scanning PZTs, the repumping signal is clearly observed. Fluorescence is maximally increased by 40% when two lasers are both on resonance and offer sufficient power, so a higher atomic density in the blue MOT is realized. $^3P_2$-$^3S_1$ and $^3P_0$-$^3S_1$ transitions in ^{84}Sr have been roughly measured to be 423913460 (30, sys.) (6, stat.) MHz and 441332834 (30, sys.) (3, stat.) MHz respectively. In addition, another main purpose

of employing two repump lasers is to deplete the population in the two metastable states induced by the transparency beam in the red MOT of the SrPAL machine, and thus restore the red MOT. During the course of this thesis, this goal has been achieved and further development of the machine has been in progress.

Chapter 4 describes construction of an iodine spectroscopy, which we hope will act as a general wavemeter for our lab's lasers. The wavelengths we are currently interested in include 679.289 nm, 707.202 nm (two repumping transitions in Sr) and 671.206 nm ($^1S_0$-$^3P_2$ clock transition). This spectral region in the iodine molecule has not been well studied in literature. The reason may be that this region involves transitions whose lower state is not the ground-state and a very high temperature is required for sufficient population, and also there was not so much need to explore it in the past. The temperature we would like to reach is above 400 K while our cell initially only made it to 250 °C. Therefore, it was decided to further thermally insulate the cell's housing by foil resulting in a shorting of electronics inside the cell. The optical setup is almost finished except for the newly conceived telescopes.

5.2 Outlook

The current ECDL design can provide reasonably good stability. Clearly, further improvement is possible, especially in the design of the base and the grating mount. Now, sizes of both the base and the grating mount are still bigger than actually needed, so more space can be spared for cables to lessen engineering chores. Additionally, the bolting holes for the grating mount cannot offer a wide range of Littrow angle. So a more general design covering a wide spectral range may be a good improvement.

For the repump laser setup, an absolute frequency reference is now absent and should be implemented in the future. As explained in chapter 3, a hollow cathode lamp is able to offer good population in the two metastable states for a strontium cell and has already been used in various groups (JILA [24], MPQ [25]). For the two repumping transitions (MHz linewidth for both), an absolute frequency locking is advantageous as the Pound-Drever-Hall scheme is technically more complex and the associated linewidth reduction is not very essential for any MHz-linewidth transition.

Now the iodine cell suffers from electronic problems. If the problem is fixed in the future, the iodine spectroscopy is worth studying in the spectral range of interest so that it can offer absolute frequency reference for all the lasers in our lab. Also, two telescopes should be implemented in the future to cover the full cross-section of the glass cell's optical entrance.

Acknowledgement

Working in a quantum gas lab is a whole new wonderful journey for me. And there are so many people I owe and I want to acknowledge.

First of all, I would like to express my sincere gratitude to Prof. Florian Schreck and Prof. Ronald Hanson. I thank Florian for giving me the chance to work in his lab. His careful reading of my thesis and comments are greatly appreciated. I wish him and his lab the best in the future and surely he will make it. Also, I thank Ronald for agreeing to become my supervisor in the master project. His help is crucial for me.

I would also like to express my sincere gratitude to my daily supervisors Shayne Bennetts and Chun-Chia Chen. Shayne designed the new-version base, a new piece of Lego for me to continue my Lego building of the two ECDLs. Chun-Chia made the old PI controller for laser locking, which comes from Jook's treasure chest, great again. He also contributed significantly to the laser setup construction. I learned a lot from the afternoon lesson &test by Shayne and the hand-by-hand dirty-work training by Chun-Chia. Their care and patience on me are essential. I will never forget the time working with them.

I also want to thank Benjamin Pasquiou for building the locking cavity setup, Oleksiy Onishchenko for the discussions and collaboration on the building of the iodine spectroscopy, the rest of the SrBEC team and the Atom-Ion guys for their generous help.

Finally, I want to thank my beloved parents. Your love and support are invaluable in my life.

Bibliography

[1] https://en.wikipedia.org/wiki/File:Simple_qw_laser_diode.svg.

[2] https://commons.wikimedia.org/wiki/File:Diode_laser.jpg.

[3] https://commons.wikimedia.org/wiki/File:Laser_diode_chip.jpg.

[4] W. Ketterle, *Happy birthday BEC*, Nature Phys. **11**, 982 (2015).

[5] R. Paschotta, *Encyclopedia of Laser Physics and Technology*, https://www.rp-photonics.com/encyclopedia.html.

[6] T. L. Nicholson, S. L. Campbell, R. B. Hutson, G. E. Marti, B. J. Bloom, R. L. McNally, W. Zhang, M. D. Barrett, M. S. Safronova, G. F. Strouse, W. L. Tew & J. Ye, *Systematic evaluation of an atomic clock at* 2×10^{-18} *total uncertainty*, Nat. Commun. **6**, 6896 (2015).

[7] M. M. Boyd, *High Precision Spectroscopy of Strontium in an Optical Lattice: Towards a New Standard for Frequency and Time*, Ph.D. thesis, University of Colorado at Boulder, 2007.

[8] M. Yasuda, H. Katori, *Lifetime Measurement of the* $^3P_2$ *Metastable State of Strontium Atoms*, Phys. Rev. Lett. **92**, 153004 (2004).

[9] H. Katori, T. Ido, Y. Isoya, and M. Kuwata-Gonokami, *Magneto-Optical Trapping and Cooling of Strontium Atoms Down to the Photon Recoil Temperature*, Phys. Rev. Lett. **82**, 1116 (1999).

[10] S. Stellmer, M. K. Tey, B. Huang, R. Grimm, and F. Schreck, *Bose-Einstein Condensation of Strontium*, Phys. Rev. Lett. **103**, 200401 (2009).

[11] S. Bennetts, C. C. Chen, B. Pasquiou, F. Schreck, *Steady-state magneto-optical trap with a phase-space density of* 10^{-3}, 2017, (eprint arXiv:1706.04689).

[12] S. Stellmer, B. Pasquiou, R. Grimm, and F. Schreck, *Laser Cooling to Quantum Degeneracy*, Phys. Rev. Lett. **110**, 263003 (2013).

[13] SrBEC webpage, `http://www.strontiumbec.com`.

[14] X. Xu, T. H. Loftus, J. L. Hall, A. Gallagher, and J. Ye, *Cooling and trapping of atomic strontium*, J. Opt. Soc. Am. B **20**, 968 (2003).

[15] T. B. M. van Leent, *Narrow-linewidth External Cavity Diode Lasers for Atomic Physics*, Master thesis, University of Amsterdam, 2017.

[16] L. Ricci, M. Weidemüller, T. Esslinger A. Hemmerich, C. Zimmermann, V. Vuletic, W. König, T. W. Hänsch, *A compact grating-stabilized diode laser system for atomic physics*, Opt. Commun. **117**, 541 (1995).

[17] S. D. Saliba, R. E. Scholten, *Linewidths below 100 kHz with external cavity diode lasers*, Appl. Opt. **48**, 6961 (2009).

[18] MOGlab, *External Cavity Diode Laser Model ECD004*, `http://www.moglabs.com/uploads/2/4/2/1/24212474/manual_ecd004_rev423.pdf`.

[19] `https://www.intl-lighttech.com/support/manipulating-light-chapter-4-light-measurement-tutorial`.

[20] H. Loh, Y. J. Lin, I. Teper, M. Cetina, J. Simon, J. K. Thompson, and V. Vuletić, *Influence of grating parameters on the linewidths of external-cavity diode lasers*, Appl. Opt. **45**, 9191 (2006).

[21] `https://www.thorlabs.com/newgrouppage9.cfm?objectgroup_id=25`.

[22] L. Nilse, H. J. Davies, and C. S. Adams, *Synchronous tuning of extended cavity diode lasers: the case for an optimum pivot point*, Appl. Opt. **38**, 548 (1999).

[23] J. L. Hall, M. S. Taubman, J. Ye, in *Handbook of Optics Volumn 4*, edited by M. Bass, J. M. Enoch, E. W. Van Stryland, W. L. Wolfe (McGraw-Hill, New York, 2000), pp. 27.1-27.24.

[24] M. A. Norcia and J. K. Thompson, *Simple laser stabilization to the strontium ^{88}Sr transition at 707 nm*, Rev. Sci. Instrum. **87**, 023110 (2016).

[25] R. G. Escudero, *Magnetic Field Control and Laser Frequency Stabilization for Strontium Magneto-Optical Traps*, Master thesis, Ludwig Maximilians Universität München, 2016.

[26] E. D. Black, *An introduction to Pound–Drever–Hall laser frequency stabilization*, Am. J. Phys. **69**, 79 (2001).

[27] J. L. Hall, L. Hollberg, T. Baer, and H. G. Robinson, *Optical heterodyne saturation spectroscopy*, Appl. Phys. Lett. **39**, 680 (1981).

[28] S. Stellmer, *Degenerate quantum gases of strontium*, Ph.D. thesis, University of Innsbruck, 2012.

[29] S. Stellmer, F. Schreck, *Reservoir spectroscopy of* $5s5p\ ^3P_2$–$5snd\ ^3D_{1,2,3}$ *transitions in strontium*, Phys. Rev. A **90**, 022512 (2014).

[30] J. E. Sansonetti, G. Nave, *Wavelengths, transition probabilities, and energy levels for the spectrum of neutral strontium (Sr I)*, J. Phys. Chem. Ref. Data **39**, 033103 (2010).

[31] Y. C. Huang, H. C. Chen, S. E. Chen, J. T. Shy, and L. B. Wang, *Precise frequency measurements of iodine hyperfine transitions at 671 nm*, Appl. Opt. **52**, 1448 (2013).

[32] L. S. Chen, *High-Precision Spectroscopy of Molecular Iodine: From Optical Frequency Standards to Global Descriptions of Hyperfine Interactions and Associated Electronic Structure*, Ph.D. thesis, University of Colorado at Boulder, 2005.

[33] J. Ye, L. S. Ma, and J. L. Hall, *Molecular Iodine Clock*, Phys. Rev. Lett. **87**, 270801 (2001).

[34] G. C. Bjorklund and M. D. Levenson, *Sub-Doppler frequency-modulation spectroscopy of I_2*, Phys. Rev. A **24**, 166 (1981).

[35] A. Dareau, M. Scholl, Q. Beaufils, D. Döring, J. Beugnon, and F. Gerbier, *Doppler spectroscopy of an ytterbium Bose-Einstein condensate on the clock transition*, Phys. Rev. A **91**, 023626 (2015).

[36] Y. C. Hsiao, C. Y. Kao, H. C. Chen, S. E. Chen, J. L. Peng, and L. B. Wang, *Absolute frequency measurement of the molecular iodine hyperfine transitions at 548 nm*, J. Opt. Soc. Am. **30**, 328 (2013).

[37] A. D. Ludlow, *The Strontium Optical Lattice Clock: Optical Spectroscopy with Sub-Hertz Accuracy*, Ph.D. thesis, University of Colorado at Boulder, 2008.

[38] A. V. Taichenachev, V. I. Yudin, C. W. Oates, C. W. Hoyt, Z. W. Barber, and L. Hollberg, *Magnetic Field-Induced Spectroscopy of Forbidden Optical Transitions with Application to Lattice-Based Optical Atomic Clocks*, Phys. Rev. Lett. **96**, 083001 (2006).

[39] *Saturated Absorption Spectroscopy*, `http://www.phys.ufl.edu/courses/phy4803L/group_III/sat_absorbtion/SatAbs.pdf`.

[40] G. Grynberg, A. Aspect, C. Fabre, *Introduction to Quantum Optics: From the Semi-classical Approach to Quantized Light* (Cambridge University Press, 2010).

[41] T. Rieger and T. Volz, *Doppler-Free Saturation Spectroscopy*, `https://www.mpq.mpg.de/4992695/saturation_spectroscopy.pdf`.